energies

Article

Subdomain Analytical Modeling of a Double-Stator Spoke-Type Permanent Magnet Vernier Machine

Xiangdong Su [1], Hang Zhao [1,*], Zhijun Ou [1], Jincheng Yu [2] and Chunhua Liu [3]

[1] Robotics and Autonomous Systems Thrust, The Hong Kong University of Science and Technology (Guangzhou), Guangzhou 511453, China; xsu847@connect.hkust-gz.edu.cn (X.S.); zhijunou@hkust-gz.edu.cn (Z.O.)
[2] School of Mechanical Engineering and Automation, Harbin Institute of Technology (Shenzhen), Shenzhen 518055, China; yujincheng@hit.edu.cn
[3] School of Energy and Environment, City University of Hong Kong, Hong Kong 999077, China
* Correspondence: hangzhao@hkust-gz.edu.cn

Abstract: This paper proposes an analytical model of the double-stator spoke-type permanent magnet vernier machine (DSSTVM) using the subdomain method (SDM), which can be used to calculate the magnetic field distribution and corresponding electromagnetic parameters of the DSSTVM. The whole field domain is divided into several subdomains according to the magnetic characteristics of each region, within which Laplace's and Poisson's equations are solved accordingly in terms of magnetic vector potential (MVP). Then, the corresponding magnetic flux density distribution, back electromotive force (EMF), and electromagnetic torque of the DSSTVM can be obtained. Ultimately, finite element analysis (FEA) is adopted to validate the proposed analytical model's effectiveness for quickly predicting the no-load and on-load performances of the DSSTVM.

Keywords: finite element analysis; subdomain method; spoke-type permanent magnet; double-stator machine; vernier machine

check for updates

Citation: Su, X.; Zhao, H.; Ou, Z.; Yu, J.; Liu, C. Subdomain Analytical Modeling of a Double-Stator Spoke-Type Permanent Magnet Vernier Machine. *Energies* **2024**, *17*, 1114. https://doi.org/10.3390/en17051114

Academic Editor: Frede Blaabjerg

Received: 23 December 2023
Revised: 15 February 2024
Accepted: 22 February 2024
Published: 26 February 2024

1. Introduction

Compared to conventional single-stator electric machines, double-stator machines (DSMs) have the merits of a more compact structure, higher torque/power density, and better fault-tolerant capability [1]. Due to these advantages, DSMs have great potential to be applied in torque-sensitive scenarios, such as wind turbines, ship propulsion motors, robot actuators, etc. [2]. With the development of manufacturing technology, DSMs have recently become a research hot spot, and various types of DSMs have been proposed, including DS flux-switching machines [3,4], DS synchronous machines [5], DS-switched reluctance machines [6], and DS vernier machines. The prominent feature of DSMs is the double-stator structure, where two stators sandwich the rotor at the inner and outer sides. Thus, DSMs can effectively use the magnetic force at both air gaps to produce a large torque.

Among all the DSM topologies, DS vernier machines have the largest torque density due to the use of the magnetic-gearing effect [7,8], but a relatively low power factor. A DS vernier machine topology was raised in [9], and the low power factor problem can be solved with the introduction of spoke-type permanent magnets. This motor topology is named a double-stator spoke-type permanent magnet vernier machine (DSSTVM), and it shows great promise in low-speed direct-drive applications.

However, the electromagnetic performance prediction for this DSSTVM is never an easy task. In general, the difficulties of the DSSTVM's field prediction come in two aspects. The first one is the dual air-gap structure. The second is plenty of effective spatial harmonics within the DSSTVM to generate such a large output torque. Electromagnetic field calculation based on finite element analysis (FEA) is the most popular and mature research method, it can accurately calculate the electromagnetic field of the electrical machines. FEA has good geometric adaptability, however, the FEA model for the DSSTVM should have a very dense mesh to accurately calculate its electromagnetic field distribution and key electromagnetic parameters. The large-scale FEA requires high computer hardware and takes a long time to model and calculate, while SDM can realize the electromagnetic field calculation of DSSTVM at a lower cost, it is used to realize the fast and accurate prediction of the electromagnetic scheme of DSSTVM. Considering the complex harmonic magnetic flux density in the vernier motor, the FEA model needs a denser mesh and smaller time step to describe the sensitive and saturated magnetic flux density distribution, while the SDM has a lower computation cost when describing the more precise characterization of electromagnetic fields. In conclusion, FEA can accurately calculate the electromagnetic field of electrical machines. However, the FEA model for the DSSTVM should have a very dense mesh to accurately calculate its electromagnetic parameters, which significantly reduces the computation speed.

An alternative to FEA used for the preliminary design of electric machines is the analytical modeling method. Up to now, various analytical modeling methods have been proposed based on different mathematical theories. Three analytical modeling methods have been frequently used for the field prediction of various electric machines, namely the conformal mapping method (CMM), magnetic equivalent circuit method (MEC), and subdomain method (SDM). CMM can be used for single-rotor electric machines with two different magnetic potentials [10], and the sliding mesh modeling is very complicated in MEC [11,12]. Thus, neither CMM nor MEC is feasible for the field prediction of DSSTVM. SDM is a semi-analytical modeling method that utilizes the Fourier series expansion to satisfy magnetic field distribution within electric machines [13]. It has the advantages of high accuracy and fast computation speed, and it is highly suitable for modeling vernier machines where plenty of spatial harmonics exist [14]. In summary, compared with CMM, SDM consumes less time than CMM; when considering plenty of spatial harmonics in vernier machines, SDM has the greater advantage in computation speed. Compared with MEC, SDM is easy for physical and mathematical modeling and consequent programming, and it does not need the complicated sliding mesh modeling. However, in the literature, there is little concerning the SDM for DSM. The magnetic field of a consequent-pole DSM is solved using SDM in [15], but the mathematical modeling of open slot structure, split-tooth structure, and spoke-type PMs are not involved.

This paper provides an SDM model for the field prediction of the DSSTVM with a split tooth structure. The modeling deduction is a supplement to [15]. Thereafter, SDM can be completed to be used for magnetic field predictions of DSMs with any topologies and pole-slot combinations. Finally, the proposed SDM model is verified by FEA software JMAG-Designer 22.0.

2. Machine Geometry and Methodology

The studied DSSTVM is composed of three components, namely a rotor, an open-slot outer stator, and a split-tooth inner stator with axial length L, as depicted in Figure 1a, and its winding configuration is shown in Figure 1b. In this DSSTVM, its rotor's permanent magnets (PMs) pole-pair number, the pole-pair numbers of the inner and outer stators' windings, and the slot numbers of the inner and outer stators are represented by P_r, P_w, and Z, respectively. To output a relatively large torque, this DSSTVM should obey the basic flux modulation principle of vernier machines [16]. Hence, the relation among P_r, P_w, and Z is governed by:

$$P_w = Z - P_r \tag{1}$$

The values of the geometrical parameters for the studied DSSTVM are provided in Table 1. All the sides of the machine's geometry are parallel to the axes of the polar coordinates to simplify the modeling process. Additionally, a few assumptions are settled before the detailed modeling process: (1) the permeability of silicon steel is regarded as infinite; (2) the axial-direction magnetic field is ignored.

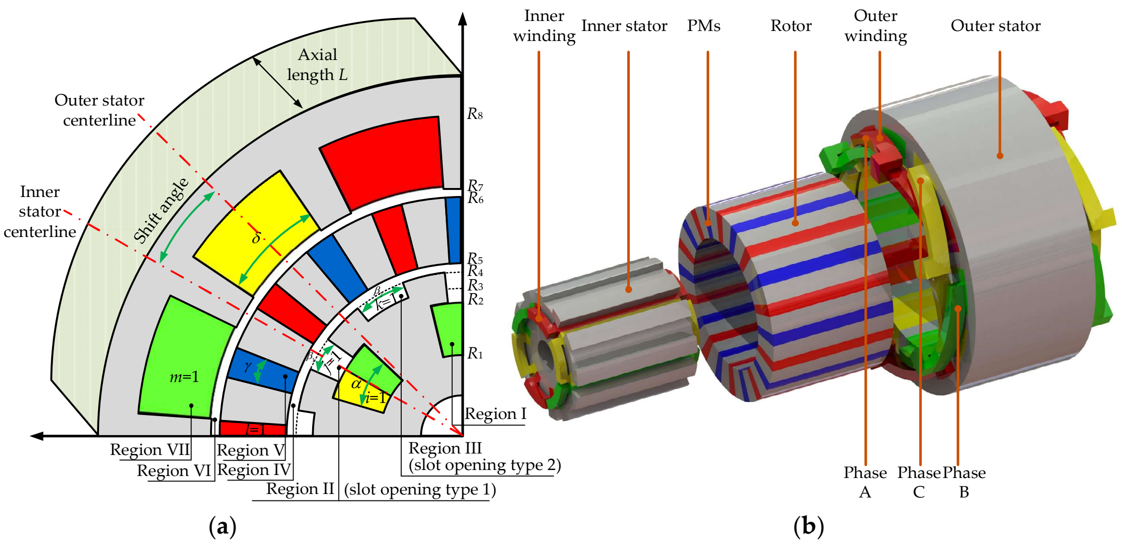

Figure 1. DSSTVM topology. (**a**) Subdomain division parameters and shift angle definition in the studied DSSTVM; (**b**) 3D scheme and winding configuration of the studied DSSTVM.

Table 1. Geometrical Parameters of The Studied DSSTVM.

Symbol	Value	Symbol	Value
R_1	24.8 mm	α	$\pi/6$ rad
R_2	41 mm	β_1	$\pi/9$ rad
R_3	45.3 mm	β_2	$\pi/10$ rad
R_4	50.3 mm	γ	$37\pi/900$ rad
R_5	50.9 mm	δ	$37\pi/300$ rad
R_6	66 mm	P_r	10
R_7	75.2 mm	P_w	2
N	200	Z	12
L	100 mm	J_z	6 A/mm^2

To solve the magnetic field within the DSSTVM, one can first divide the whole field domain into seven subdomains, namely the inner stator slot, slot-opening type 1, slot-opening type 2, inner air gap, rotor slot, outer air gap, and outer stator slot. Then, the magnetic field distribution within each region should follow Maxwell's equation. By adopting magnetic vector potential (MVP) A_z in the polar coordinates and considering various materials' properties, one can obtain the general expressions as follows [17]:

$$\frac{\partial A_z}{\partial r^2}+\frac{1}{r}\frac{\partial A_z}{\partial r}+\frac{1}{r^2}\frac{\partial A_z}{\partial \theta^2}=-\frac{\mu_0}{r}\left(\frac{\partial (r\cdot M_\theta)}{\partial r}-\frac{\partial M_r}{\partial \theta}\right)-\mu_0 J_z \tag{2}$$

where M_r and M_θ are the magnetizations in the radial and tangential directions, respectively, J_z is the current density in the z-direction, and μ_0 is the magnetic permeability in vacuum.

Both Region I and VII only contain electrified conductors, so (2) can be transferred into a Poisson's equation where the magnetization term is eliminated. Region V only contains the tangential magnetization, so (2) can be transferred into another Poisson's equation where the radial magnetization term and the current term are eliminated. As for the rest regions, they contain nothing but air, so (2) can be simplified into Laplace's equation.

The general solution of (2) is the sum of a particular integral and its complementary solution. Using the method of separation of variables, the complementary solution to (2) can be written as (The detailed derivation can be found in Appendix A):

$$\begin{aligned} A_z(r,\theta) &= (A_0+B_0\ln r)(C_0\theta+D_0) \\ &+\sum_{n=1}^{\infty}(A_n r^n+B_n r^{-n})(C_n\cos n\theta+D_n\sin n\theta) \end{aligned} \tag{3}$$

where A_0, B_0, C_0, D_0, A_n, B_n, C_n and D_n are the Fourier coefficients to be determined through the satisfaction of the boundary conditions in Section 3; n is the harmonic order in the Fourier series, and the maximum number of harmonics used in the calculation is represented by N. Then, the expression of a particular integral varies with the right side of (2), and it will be discussed case by case in the following section.

Additionally, two notations, namely $P_w(u, v)$ and $E_w(u, v)$, are introduced to simplify the expressions of the general solutions [18]:

$$P_w(u, v) = \left(\frac{u}{v}\right)^w + \left(\frac{v}{u}\right)^w \tag{4}$$

$$E_w(u, v) = \left(\frac{u}{v}\right)^w - \left(\frac{v}{u}\right)^w \tag{5}$$

3. Analytical Modeling Process

3.1. Boundary Condition and General Solution Expressions

There are three kinds of boundary conditions within the DSSTVM, namely periodic condition, continuous condition, and Neumann condition [18]: In the air gap region, MVP has a period of 2π; at the interfaces between two regions, MVP A_Z should be continuous; while the tangential component of the magnetic field intensity H should be continuous. Considering that the permeability of iron cores is regarded as infinite, the tangential component of H should be zero at the interface between the iron core and the region with other materials. With the above continuity rules, the boundary conditions of the DSSTVM will be determined from the innermost region to the outermost one subsequently. The flow chart of the analytical modeling process in this article is as shown in Figure 2.

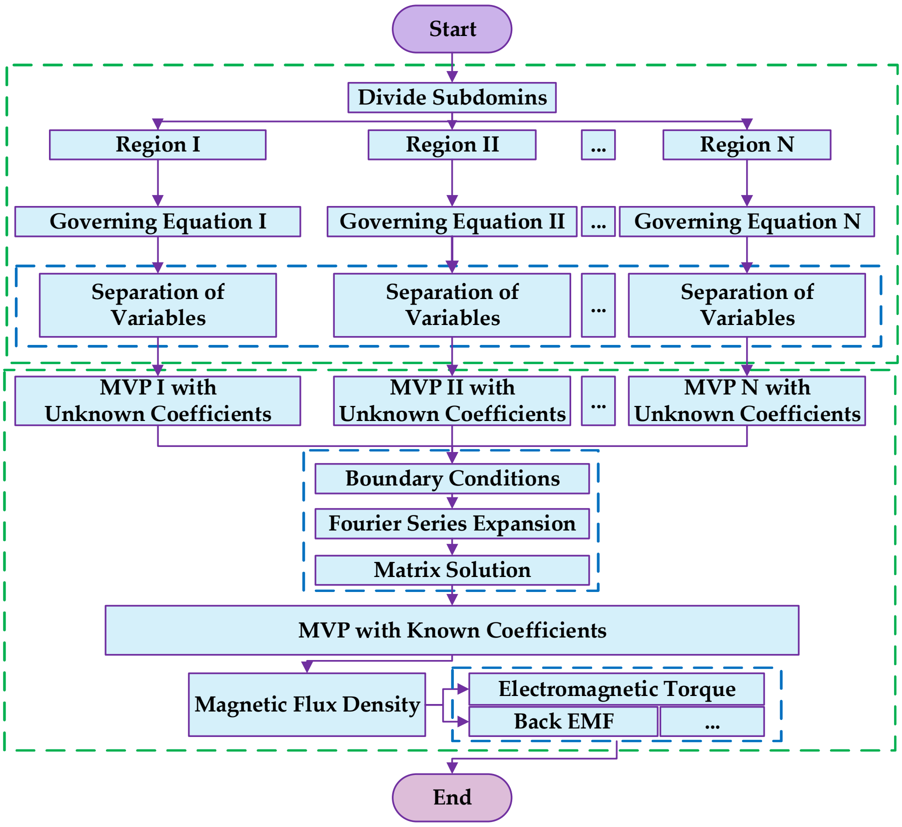

Figure 2. Flow chart of the proposed method.

3.1.1. Region I

First, the three sides surrounding the ith slot within Region I are connected to the iron core, where the tangential component of the magnetic field is zero. These features lead to:

$$\begin{cases} \left.\frac{\partial A_{I,i}}{\partial r}\right|_{r=R_1} = 0; & \theta \in [\theta_i, \theta_i + \alpha] \\ \left.\frac{\partial A_{I,i}}{\partial \theta}\right|_{\theta_i} = 0 \& \left.\frac{\partial A_{I,i}}{\partial \theta}\right|_{\theta_i+\alpha} = 0; \ r \in [R_1, R_2] \end{cases} \tag{6}$$

where $A_{I,i}$ is the MVP of the ith slot in Region I, θ_i is the initial angle of the ith slot in Region I, and α is the angle of ith slot within Region I.

The remaining upper side of Region I is connected to both the iron core and Region II. For the arc that corresponds to the iron core, the tangential component of the magnetic field is zero, while for the arc that corresponds to Region II, the tangential component of the magnetic field is continuous between Region I and Region II, so we can obtain the following boundary condition:

$$\left.\frac{\partial A_{I,i}}{\partial r}\right|_{r=R_2} = \begin{cases} \left.\frac{\partial A_{II,j}}{\partial r}\right|_{r=R_2} & \theta \in [\theta_j, \theta_j + \beta_1] \\ 0 & elsewhere \end{cases} \quad \text{with } i = j \tag{7}$$

Considering the boundary conditions in (6) and (7), the general solution of the MVP and the corresponding Fourier series coefficient in Region I can be expressed as:

$$\begin{aligned} A_{I,i}(r,\theta) &= A_0^i + \tfrac{1}{2}\mu_0 J_{i0}\left(R_1^2 \ln r - \tfrac{1}{2}r^2\right) \\ &+ \sum_{n_1=1}^{\infty} \frac{A_{n_1}^i \alpha R_2}{n_1 \pi} \frac{P_{n_1\pi/\alpha}(r,R_1)}{E_{n_1\pi/\alpha}(R_2,R_1)} \cos\left(\tfrac{n_1\pi}{\alpha}(\theta-\theta_i)\right) \\ &+ \sum_{n_1=1}^{\infty} \begin{pmatrix} \frac{2\alpha}{n_1\pi} \frac{R_1^2 P_{n_1\pi/\alpha}(r,R_2) - R_2^2 P_{n_1\pi/\alpha}(r,R_1)}{E_{n_1\pi/\alpha}(R_2,R_1)} + r^2 \\ \cdot \frac{\mu_0 J_{in}}{(n_1\pi/\alpha)^2 - 4} \cdot \cos\left(\tfrac{n_1\pi}{\alpha}(\theta-\theta_i)\right) \end{pmatrix} \end{aligned} \tag{8}$$

where

$$A_{n_1}^i = \frac{2}{\alpha} \int_{\theta_j}^{\theta_j+\beta_1} \left.\frac{\partial A_{II,j}}{\partial r}\right|_{r=R_2} \cos\frac{n_1\pi}{\alpha}(\theta-\theta_i) d\theta \tag{9}$$

3.1.2. Region II

Secondly, for the jth slot of Region II, its two lateral sides are connected to the iron core, while the lower and upper sides are connected to the ith slot of Region I and IV, respectively. Thus, the boundary conditions can be deduced as:

$$\left.\frac{\partial A_{II,j}}{\partial \theta}\right|_{\theta_j} = 0\,; \quad \left.\frac{\partial A_{II,j}}{\partial \theta}\right|_{\theta_j+\beta_1} = 0 \text{ with } r \in [R_2, R_4] \tag{10}$$

$$\begin{matrix} A_{II,j}(R_2,\theta) = A_{I,i}(R_2,\theta) \\ \theta \in [\theta_j, \theta_j+\beta_1] \end{matrix} ; \begin{matrix} A_{II,j}(R_4,\theta) = A_{IV}(R_4,\theta) \\ \theta \in [\theta_j, \theta_j+\beta_1] \end{matrix} \tag{11}$$

where $A_{II,j}$ is the MVP of the jth slot within Region II, θ_j is the initial angle of the jth slot within Region II, and β_1 is the angle of jth slot within Region II (slot-opening type 1).

Combining the boundary conditions in (10) and (11), the general solution of MVP and the corresponding Fourier series coefficient in Region II can be given by:

$$\begin{aligned} A_{II,j} \quad & (r,\theta) = A_0^j + B_0^j \ln r \\ & + \sum_{n_2=1}^{\infty} \left(A_{n_2}^j \frac{E_{n_2\pi/\beta_1}(r,R_4)}{E_{n_2\pi/\beta_1}(R_2,R_4)} - B_{n_2}^j \frac{E_{n_2\pi/\beta_1}(r,R_2)}{E_{n_2\pi/\beta_1}(R_2,R_4)} \right) \cos\left(\tfrac{n_2\pi}{\beta_1}(\theta-\theta_j)\right) \end{aligned} \tag{12}$$

where

$$A_0^j + B_0^j \ln R_2 = \frac{1}{\beta_1} \int\limits_{\theta_i + \frac{\alpha-\beta_1}{2}}^{\theta_i + \frac{\alpha+\beta_1}{2}} A_{I,i}(R_2, \theta) d\theta \tag{13}$$

$$A_0^j + B_0^j \ln R_4 = \frac{1}{\beta_1} \int\limits_{\theta_i + \frac{\alpha-\beta_1}{2}}^{\theta_i + \frac{\alpha+\beta_1}{2}} A_{IV}(R_4, \theta) d\theta \tag{14}$$

$$A_{n_2}^j = \frac{2}{\beta_1} \int\limits_{\theta_j}^{\theta_j+\beta_1} A_{I,i}(R_2, \theta) \cos(\frac{n_2 \pi}{\beta_1}(\theta - \theta_j)) d\theta \tag{15}$$

$$B_{n_2}^j = \frac{2}{\beta_1} \int\limits_{\theta_j}^{\theta_j+\beta_1} A_{IV}(R_4, \theta) \cos(\frac{n_2 \pi}{\beta_1}(\theta - \theta_j)) d\theta \tag{16}$$

3.1.3. Region III

Next, for the kth slot belonging to Region III, its three sides are connected to the iron core, where the tangential component of the magnetic field should be zero. The remaining upper side is connected to Region IV, so the MVPs of Regions III and IV are continuous at the upper side. Hence, the boundary conditions can be represented as:

$$\begin{cases} \frac{\partial A_{III,k}}{\partial \theta}\Big|_{\theta_k} = 0 \\ \frac{\partial A_{III,k}}{\partial \theta}\Big|_{\theta_k+\beta_2} = 0 \end{cases}, r \in [R_3, R_4] \; ; \; \begin{matrix} \frac{\partial A_{III,k}}{\partial r}\Big|_{r=R_3} = 0 \\ \theta \in [\theta_k, \theta_k + \beta_2] \end{matrix} \tag{17}$$

$$A_{III,k}(R_4, \theta) = A_{IV}(R_4, \theta) \text{ with } \theta \in [\theta_k, \theta_k + \beta_2] \tag{18}$$

where $A_{III,k}$ is the MVP of the kth slot within Region III, θ_k is the initial angle of the kth slot within Region III, β_2 is the angle of kth slot within Region III (slot-opening type 2).

Taking into account boundary conditions (17) and (18), the general solution of MVP and the corresponding Fourier series coefficient in Region III can be acquired as:

$$A_{III,k}(r, \theta) = A_0^k + \sum_{n_3=1}^{\infty} A_{n_3}^k \frac{P_{n_3\pi/\beta_2}(r, R_4)}{P_{n_3\pi/\beta_2}(R_3, R_4)} \cos\left(\frac{n_3 \pi}{\beta_2}(\theta - \theta_k)\right) \tag{19}$$

where

$$A_{n_3}^k = \frac{2}{\beta} \int_{\theta_k}^{\theta_k+\beta_2} A_{IV}(R_4, \theta) \cos(\frac{n_3 \pi}{\beta_2}(\theta - \theta_k)) d\theta \tag{20}$$

3.1.4. Region IV

Then, the boundary conditions for Region IV are more complicated since Region IV is adjacent to Regions II, III, and V and the iron core. We use the continuity of the tangential component of the magnetic field and handle the boundary condition by introducing a piecewise function as follows:

$$\frac{\partial A_{IV}}{\partial r}\Big|_{r=R_4} = f_1(\theta) = \begin{cases} \frac{\partial A_{II,j}}{\partial r}\Big|_{r=R_4} & \theta \in [\theta_j, \theta_j + \beta_1] \\ \frac{\partial A_{III,k}}{\partial r}\Big|_{r=R_4} & \theta \in [\theta_k, \theta_k + \beta_2] \\ 0 & elsewhere \end{cases} \tag{21}$$

$$\frac{\partial A_{IV}}{\partial r}\Big|_{r=R_5} = f_2(\theta) = \begin{cases} \frac{\partial A_{V,l}}{\partial r}\Big|_{r=R_5} + \mu_0 M_{\theta,l} & \theta \in [\theta_l, \theta_l + \gamma] \\ 0 & elsewhere \end{cases} \tag{22}$$

where A_{IV} is the MVP within Region IV, $M_{\theta,l}$ is the tangential magnetization of the lth PM within Region V, θ_l is the initial angle of the lth PM within Region V, and γ is the angle of the lth PM within Region V.

We take the boundary conditions in (21) and (22) into consideration, so the general solution of MVP and the corresponding Fourier series coefficient in Region IV can be written as:

$$\begin{aligned} A_{IV}(r,\theta) &= A_0^{IV} \\ &+ \sum_{n_4=1}^{\infty} \begin{array}{l} \left(A_{n_4}^{IV} \frac{R_4}{n_4} \frac{P_{n_4}(r,R_5)}{E_{n_4}(R_4,R_5)} + B_{n_4}^{IV} \frac{R_5}{n_4} \frac{P_{n_4}(r,R_4)}{E_{n_4}(R_5,R_4)} \right) \\ \cdot \cos(n\theta) \end{array} \\ &+ \sum_{n_4=1}^{\infty} \begin{array}{l} \left(C_{n_4}^{IV} \frac{R_4}{n_4} \frac{P_{n_4}(r,R_5)}{E_{n_4}(R_4,R_5)} + D_{n_4}^{IV} \frac{R_5}{n_4} \frac{P_{n_4}(r,R_4)}{E_{n_4}(R_5,R_4)} \right) \\ \cdot \sin(n\theta) \end{array} \end{aligned} \tag{23}$$

where

$$A_{n_4}^{IV} = \frac{1}{\pi}\int_0^{2\pi} f_1(\theta)\cos(n_4\theta)d\theta\,; \quad C_{n_4}^{IV} = \frac{1}{\pi}\int_0^{2\pi} f_1(\theta)\sin(n_4\theta)d\theta \tag{24}$$

$$B_{n_4}^{IV} = \frac{1}{\pi}\int_0^{2\pi} f_2(\theta)\cos(n_4\theta)d\theta\,; \quad D_{n_4}^{IV} = \frac{1}{\pi}\int_0^{2\pi} f_2(\theta)\sin(n_4\theta)d\theta \tag{25}$$

3.1.5. Region V

Subsequently, for the lth slot in Region V, its two lateral sides are adjacent to the iron core, and the lower and upper sides are adjacent to Region IV and Region VI, respectively. Hence, its boundary conditions can be written as follows:

$$\left.\frac{\partial A_{V,l}}{\partial\theta}\right|_{\theta=\theta_l} = 0\,; \quad \left.\frac{\partial A_{V,l}}{\partial\theta}\right|_{\theta=\theta_l+\gamma} = 0 \text{ with } r \in [R_5, R_6] \tag{26}$$

$$\begin{array}{c} A_{V,l}(R_5,\theta) = A_{IV}(R_5,\theta) \\ \theta \in [\theta_l, \theta_l+\gamma] \end{array} ; \begin{array}{c} A_{V,l}(R_6,\theta) = A_{VI}(R_6,\theta) \\ \theta \in [\theta_l, \theta_l+\gamma] \end{array} \tag{27}$$

where $A_{V,l}$ is the MVP of the lth PM within Region V and θ_l is the initial angle of lth PM within Region V.

Combing the boundary conditions in (26) and (27), the general solution of the MVP and the corresponding Fourier series coefficient in Region V can be obtained as:

$$\begin{aligned} A_{V,l}(r,\theta) &= A_0^l + B_0^l \ln r - \mu_0 M_{\theta,l} r \\ &+ \sum_{n_5=1}^{\infty} \begin{array}{l} \left(A_{n_5}^l \frac{E_{n_5\pi/\gamma}(r,R_6)}{E_{n_5\pi/\gamma}(R_5,R_6)} - B_{n_5}^l \frac{E_{n_5\pi/\gamma}(r,R_5)}{E_{n_5\pi/\gamma}(R_5,R_6)} \right) \\ \cdot \cos\left(\frac{n_5\pi}{\gamma}(\theta-\theta_l)\right) \end{array} \end{aligned} \tag{28}$$

where

$$A_0^l + B_0^l \ln R_5 = \frac{1}{\gamma}\int_{\theta_l}^{\theta_l+\gamma} A_{IV}(R_5,\theta)d\theta \tag{29}$$

$$A_0^l + B_0^l \ln R_6 = \frac{1}{\gamma}\int_{\theta_l}^{\theta_l+\gamma} A_{VI}(R_6,\theta)d\theta \tag{30}$$

$$A_{n_5}^l = \frac{2}{\gamma}\int_{\theta_l}^{\theta_l+\gamma} A_{IV}(R_5,\theta)\cos\left(\frac{n_5\pi}{\gamma}(\theta-\theta_l)\right)d\theta \tag{31}$$

$$B_{n_5}^{l} = \frac{2}{\gamma} \int_{\theta_l}^{\theta_l+\gamma} A_{VI}(R_6,\theta) \cos\left(\frac{n_5\pi}{\gamma}(\theta-\theta_l)\right) d\theta \tag{32}$$

3.1.6. Region VI

Similar to the boundary conditions in Region IV, Region VI is adjacent to Region V and VII. We can write the boundary conditions for Region VI using the piecewise function as follows:

$$\left.\frac{\partial A_{VI}}{\partial r}\right|_{r=R_6} = g_1(\theta) = \begin{cases} \left.\frac{\partial A_{V,l}}{\partial r}\right|_{r=R_6} + \mu_0 M_{\theta,l} & \theta \in [\theta_l, \theta_l+\gamma] \\ 0 & elsewhere \end{cases} \tag{33}$$

$$\left.\frac{\partial A_{VI}}{\partial r}\right|_{r=R_7} = g_2(\theta) = \begin{cases} \left.\frac{\partial A_{VII,m}}{\partial r}\right|_{r=R_7} & \theta \in [\theta_m, \theta_m+\delta] \\ 0 & elsewhere \end{cases} \tag{34}$$

where A_{VI} is the MVP within Region VI, $A_{VII,m}$ is the MVP of the mth slot within Region VII, θ_m is the initial angle of mth slot within Region VII and δ is the angle of mth slot within Region VII.

Taking into account the boundary conditions (33) and (34), the general solution of MVP and the corresponding Fourier series coefficient in Region VI can be calculated as:

$$\begin{aligned} A_{VI}(r,\theta) = \;& A_0^{VI} + \sum_{n_6=1}^{\infty}\left(A_{n_6}^{VI}\frac{R_6}{n_6}\frac{P_{n_6}(r,R_7)}{E_{n_6}(R_4,R_5)} + B_{n_6}^{VI}\frac{R_7}{n_6}\frac{P_{n_6}(r,R_6)}{E_{n_6}(R_7,R_6)}\right)\cdot\cos(n\theta) \\ & + \sum_{n_6=1}^{\infty}\left(C_{n_6}^{VI}\frac{R_6}{n_6}\frac{P_{n_6}(r,R_7)}{E_{n_6}(R_4,R_5)} + D_{n_6}^{VI}\frac{R_7}{n_6}\frac{P_{n_6}(r,R_6)}{E_{n_6}(R_7,R_6)}\right)\cdot\sin(n\theta) \end{aligned} \tag{35}$$

where

$$A_{n_6}^{VI} = \frac{1}{\pi}\int_0^{2\pi} g_1(\theta)\cos(n_6\theta)d\theta\;;\quad C_{n_6}^{VI} = \frac{1}{\pi}\int_0^{2\pi} g_1(\theta)\sin(n_6\theta)d\theta \tag{36}$$

$$B_{n_6}^{VI} = \frac{1}{\pi}\int_0^{2\pi} g_2(\theta)\cos(n_6\theta)d\theta\;;\quad D_{n_6}^{VI} = \frac{1}{\pi}\int_0^{2\pi} g_2(\theta)\sin(n_6\theta)d\theta \tag{37}$$

3.1.7. Region VII

Finally, the three sides of the mth slot within Region VII are connected to the iron core, and the remaining lower side is adjacent to Region VI. Therefore, the corresponding boundary conditions can be arranged as:

$$\begin{cases} \left.\frac{\partial A_{VII,m}}{\partial \theta}\right|_{\theta_m} = 0 \\ \left.\frac{\partial A_{VII,m}}{\partial \theta}\right|_{\theta_m+\delta} = 0 \end{cases},\; r\in[R_7,R_8]\;;\; \begin{array}{l} \left.\frac{\partial A_{VII,m}}{\partial r}\right|_{r=R_8} = 0 \\ \theta\in[\theta_m,\theta_m+\delta] \end{array} \tag{38}$$

where

$$A_{VII,m}(R_7,\theta) = A_{VI}(R_7,\theta) \text{ with } \theta\in[\theta_m,\theta_m+\delta] \tag{39}$$

Considering the boundary conditions (38) and (39) together, the general solution of MVP and the corresponding Fourier series coefficient in Region VI can be written as:

$$\begin{aligned} A_{VII,m}(r,\theta) &= A_0^m + \tfrac{1}{2}\mu_0 J_m\left(R_8^2\ln r - \tfrac{1}{2}r^2\right) \\ &+ \sum_{n_7=1}^{\infty} A_{n_7}^m \frac{P_{n_7\pi/\delta}(r,R_8)}{P_{n_7\pi/\delta}(R_7,R_8)}\cos\left(\tfrac{n_7\pi}{\delta}(\theta-\theta_m)\right) \end{aligned} \tag{40}$$

where

$$A_{n_7}^m = \frac{2}{\delta} \int_{\theta_m}^{\theta_m+\delta} A_{VI}(R_7, \theta) \cos\left(\frac{n_7 \pi}{\delta}(\theta - \theta_m)\right) d\theta \tag{41}$$

The unknown Fourier series coefficients in the MVP expression and the unknown integral functions are deduced in detail in Appendices B and C, respectively. Ultimately, by combining all the Fourier series coefficient expressions of MVPs within the machine domain, we can obtain a system of linear equations with a unique solution. The Fourier series coefficients can be obtained by solving the system of linear equations in a numerical computing software, for instance, MATLAB R2022b. Subsequently, the magnetic flux density B in all these regions can be acquired according to:

$$B_r = \frac{1}{r}\frac{\partial A_z}{\partial \theta} \text{ and } B_\theta = -\frac{\partial A_z}{\partial r} \tag{42}$$

where B_r and B_θ are the radial and tangential components of magnetic flux density, respectively.

3.2. Postprocessing Electromagnetic Parameters Calculation

The output torque on the rotor of DSSTVM T_r should be the sum of electromagnetic torques on the inner air gap and outer air gap, namely T_{inner_gap} and T_{outer_gap}. Then, the electromagnetic torque on the air gap can be calculated by using the Maxwell stress tensor, which can be given as follows:

$$T_{inner\_gap} = \frac{LR_{in}^2}{\mu_0} \int_0^{2\pi} B_{IV,r}(R_{in}, \theta) B_{IV,\theta}(R_{in}, \theta) d\theta \tag{43}$$

$$T_{outer\_gap} = \frac{LR_{out}^2}{\mu_0} \int_0^{2\pi} B_{VI,r}(R_{out}, \theta) B_{VI,\theta}(R_{out}, \theta) d\theta \tag{44}$$

$$T_r = T_{inner\_gap} + T_{outer\_gap} \tag{45}$$

where R_{in} and R_{out} are the radii in the middle of the inner air gap and outer air gap.

As for the flux linkage of each coil, it can be calculated as the area integral of MVP within the slot region. Then, the phase flux can be obtained as the product of the slot-connecting matrix and the flux linkage vector. The back electromotive force (EMF) can be acquired as the derivative of the phase flux with respect to time. The detailed deduction process can be referred to [19].

4. Finite Element Analysis Validation

The DSSTVM simulation model is constructed via FEA to verify the effectiveness of the proposed SDM, and the structural parameters of the DSSTVM model are referred to in Table 1. The DSSTVM's main performance indicators are average electromagnetic torque, electromagnetic torque ripple rate, efficiency, loss, etc. The above indicators will determine the DSSTVM's output performance under different operating conditions and application scenarios. In the aspect of magnetic flux density distribution, the analytical model would provide detailed insights into how the magnetic flux density is distributed across the machine. This helps to identify areas of high flux density, potential magnetic flux leakage, and regions where saturation might occur. According to Maxwell stress tensor method in (43) and (44), the magnetic flux density distribution in the airgap is essential for the calculation of electromagnetic torque. Understanding the magnetic flux distribution is crucial for optimizing the design to maximize the efficiency and torque capability of the machine, as well as for reducing torque ripple and ensuring smooth operation. In this article, to evaluate the accuracy of the proposed method, the calculation results based on the proposed method are compared with FEA.

The no-load and on-load magnetic flux density and flux line distributions calculated by FEA are depicted in Figure 3a and Figure 3b, respectively. The no-load magnetic flux density distribution comparison between SDM and FEA in the inner and outer air gaps are illustrated in Figure 4a and Figure 4b, respectively. The harmonic spectrum of the air gap magnetic flux density in the middle of the inner air gap and outer air gap under no-load condition between SDM and FEA are illustrated in Figure 5a and Figure 5b, respectively. The rated load magnetic flux density distribution comparison between SDM and FEA in the inner and outer air gaps are illustrated in Figure 6a and Figure 6b, respectively. The harmonic spectrum of the air gap magnetic flux density in the middle of the inner air gap and outer air gap under rated load condition between SDM and FEA are illustrated in Figure 7a and Figure 7b, respectively. It can be observed that the proposed SDM has good agreement with that of FEA in terms of the magnetic flux densities and harmonic spectrum in inner and outer air gaps.

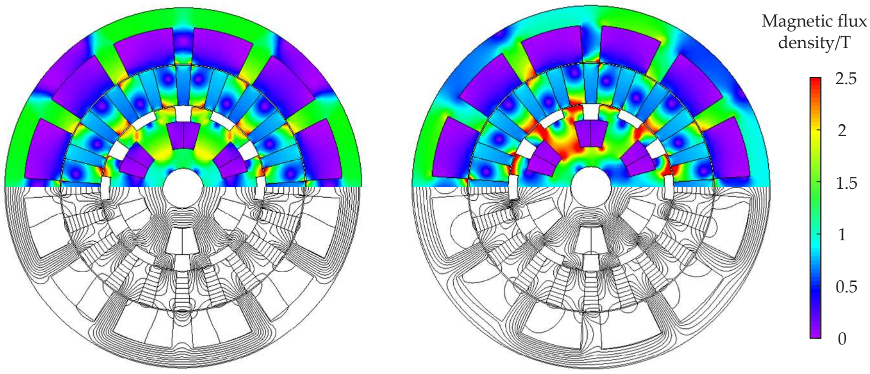

(**a**) (**b**)

Figure 3. Magnetic field distribution of the studied DSSTVM calculated by the FEA. (**a**) No-load condition; (**b**) On-load condition.

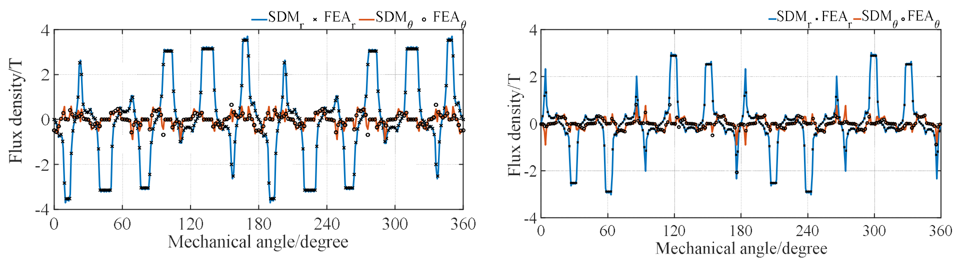

(**a**) (**b**)

Figure 4. No-load magnetic flux density distribution of the studied DSSTVM. (**a**) Radial and tangential component in the middle of the inner air gap; (**b**) Radial and tangential component in the middle of the outer air gap.

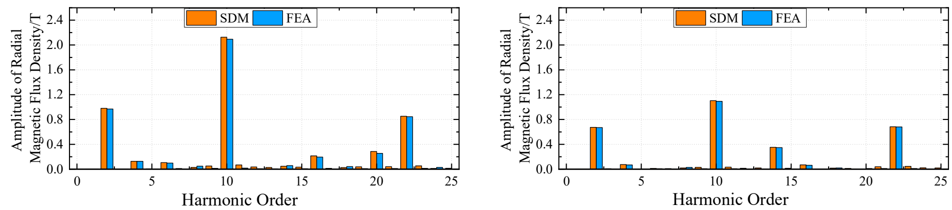

(**a**) (**b**)

Figure 5. No-load magnetic flux density distribution of the studied DSSTVM. (**a**) Harmonic spectrum of the radial component in the middle of the inner air gap; (**b**) Harmonic spectrum of the radial component in the middle of the outer air gap.

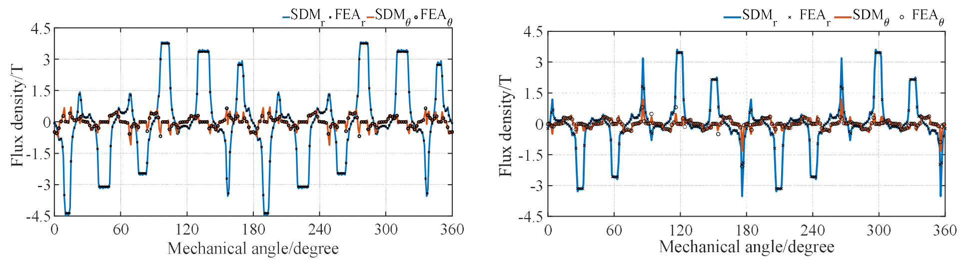

(**a**) (**b**)

Figure 6. Rated load magnetic flux density distribution of the studied DSSTVM. (**a**) Radial and tangential component in the middle of the inner air gap; (**b**) Radial and tangential component in the middle of the outer air gap.

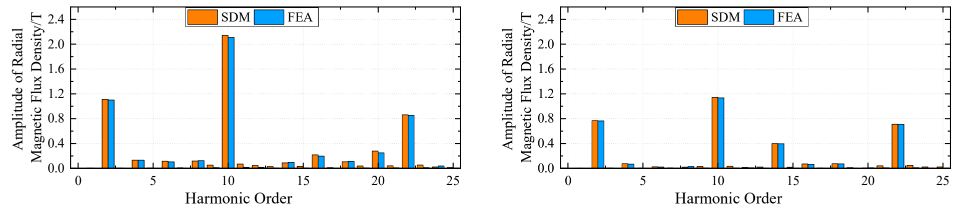

(**a**) (**b**)

Figure 7. Rated load magnetic flux density distribution of the studied DSSTVM. (**a**) Harmonic spectrum of the radial component in the middle of the inner air gap; (**b**) Harmonic spectrum of the radial component in the middle of the outer air gap.

One prominent advantage of using DSSTVM is the reduction in flux leakage, so the output torque and power factor of the machines can be greatly improved. To minimize the flux leakage of the spoke-type PMs on the rotor, one can determine the optimal shift angle between the inner and outer stators via the parameter-sweeping method, as depicted in Figure 1. This can also be achieved by using the proposed SDM, and Figure 8a illustrates the variation in the output torque and power factor with the variation in shift angle from 0 to 30 degrees, calculated by both SDM and FEA.

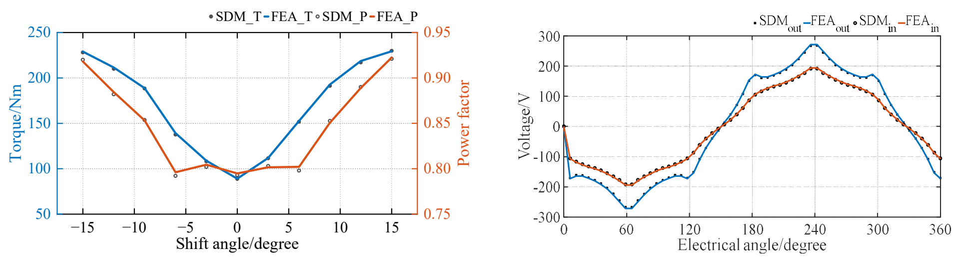

(**a**) (**b**)

Figure 8. Torque and power factor optimization of the studied DSSTVM. (**a**) Torque and power factor change with the variation in shift angle; (**b**) No-load back EMF waveforms.

No-load back EMF is one essential parameter in motor design, it is influenced by the motor's topology, the PM arrangement, etc. No-load back EMF can impact the control strategy in motor the operation. Understanding its waveform helps in designing appropriate topologies and control algorithms to achieve optimal performance. In addition, torque is another critical performance indicator for DSSTVM. The analytical model would provide the torque characteristics of the DSSTVM, including the average torque, torque ripple, and the relationship between torque and current. It helps to understand the impact of design parameters on average torque and torque ripple. Therefore, analyzing the output torque helps in optimizing the motor design for desired load conditions and ensuring that the motor generates the necessary performance for its intended application.

Therefore, the DSSTVM's no-load back EMF waveforms with different sets of windings operating can be obtained by using FEA and SDM, as can be seen in Figure 8b. The harmonic spectrum of the no-load back EMF waveforms in the inner stator and outer stator between SDM and FEA are illustrated in Figure 9a and Figure 9b, respectively. The DSSTVM's output torques with different sets of windings operating can be obtained by using FEA and SDM, as can be seen in Figure 10a. The rated load torque harmonic spectrum of the DSSTVM in mode 1 (the inner and outer parts of DSSTVM operate simultaneously to generate the torque), mode 2 (the inner part of DSSTVM operates to generate the torque), and mode 3 (the outer part of DSSTVM operate to generate the torque) between SDM and FEA are illustrated in Figure 10b, Figure 10c and Figure 10d, respectively.

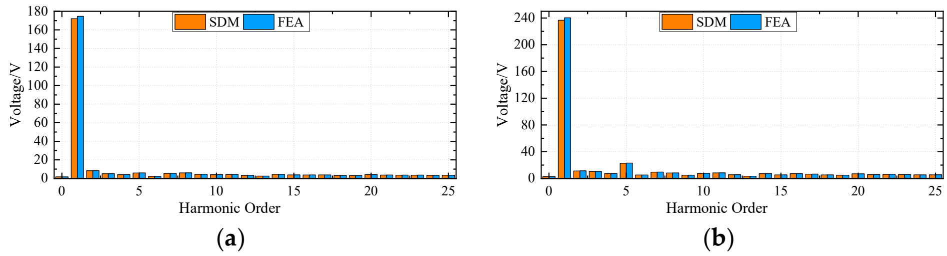

Figure 9. Harmonic spectrum of no-load back EMF waveforms of the studied DSSTVM. (**a**) Inner stator; (**b**) Outer stator.

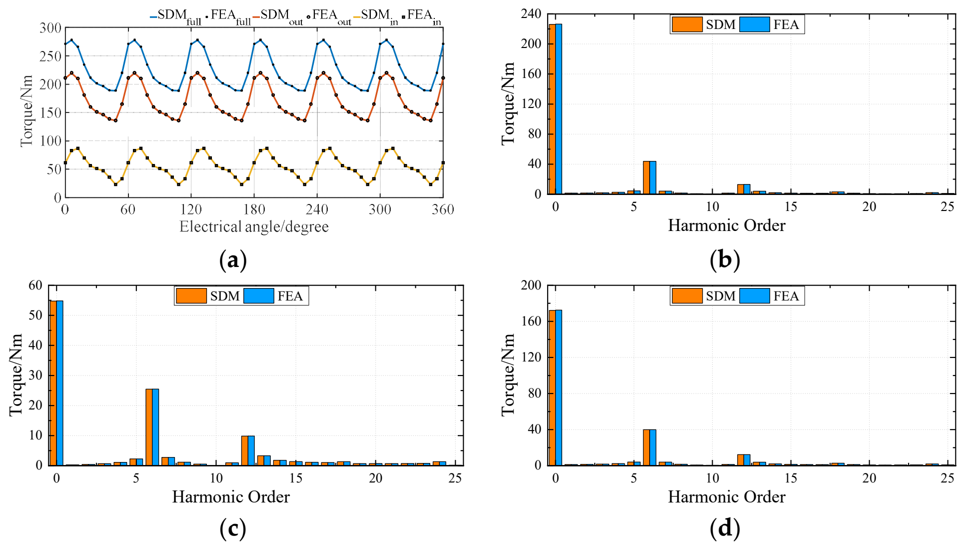

Figure 10. Rated load torque and harmonic spectrum of the studied DSSTVM. (**a**) Torque wave-forms of three different modes (mode 1, mode 2 and model 3); (**b**) Harmonic spectrum of the torque wave-form of mode 1; (**c**) Harmonic spectrum of the torque wave-form of mode 2; (**d**) Harmonic spectrum of the torque wave-form of mode 3.

In terms of the amplitude of the radial and tangential magnetic flux density in the middle of the inner air gap and outer air gap, compared with the permanent magnet synchronous motors (PMSMs), DSSTVM has a higher magnetic flux density because of the magnetic field modulation. As a result, according to the Maxwell stress tensor, the higher magnetic flux density in the airgap generates higher electromagnetic torque. Therefore, in terms of the rated load torque, in one aspect, because of the amplitude of the radial and tangential magnetic flux density in the middle of the inner air gap and outer air gap, compared with the PMSMs, DSSTVM has a higher electromagnetic torque. In another aspect, the double-stator characteristic makes the DSSTVM able to generate the electromagnetic torque from the inner and outer airgap simultaneously or separately, which makes the DSSTVM have higher electromagnetic torque density and wider application scenarios.

However, a slight deviation between the two approaches can be observed, where the values of SDM are smaller. This is due to the maximum harmonic limit of the SDM, and the error can be smaller if the calculated maximum harmonic number increases. However, the computation time increases along with the rise in the calculated maximum harmonic number, so we should make a trade-off for different application scenarios. As for the computation time, it takes the SDM 29 s for a single step, while it takes FEA 47 s. Thus, the computation time of SDM is only 62% of that of FEA, proving that the SDM is prior to being applied to the initial design stage to determine the slot-pole combinations and parameters' ranges to be optimized for DSSTVM as well as other double-stator machines.

5. Conclusions

This paper presents a high-fidelity analytical method, namely the subdomain method, for calculating the magnetic field distribution and the related electromagnetic parameters in DSSTVM. The magnetic flux density distribution, back EMF, and output torque of the DSSTVM are computed by both the SDM and FEA. Compared to FEA, the proposed SDM can save computation time while maintaining accuracy. The deduction process completes the SDM for double-stator machines with various structures as well as slot-pole combinations. This analytical method can be applied for topology investigation and optimization for double-stator machines.

Author Contributions: Conceptualization, X.S.; methodology, X.S.; software, H.Z.; validation, H.Z.; formal analysis, J.Y.; investigation, J.Y.; resources, X.S.; data curation, H.Z.; writing—original draft preparation, X.S.; writing—review and editing, C.L.; visualization, Z.O.; supervision, H.Z.; project administration, H.Z.; funding acquisition, H.Z. All authors have read and agreed to the published version of the manuscript.

Funding: This work was supported in part by the Guangdong Basic and Applied Basic Research Foundation under Project 2022A1515110361 and Guangzhou Science and Technology Bureau under Project SL2022A04J00605 and Project SL2022A03J00086.

Institutional Review Board Statement: Not applicable.

Informed Consent Statement: Not applicable.

Data Availability Statement: Data are contained within the article.

Conflicts of Interest: The authors declare no conflicts of interest.

Abbreviations

R_1	The inner radius of the inner stator slot
R_2	Inner radius of opening slot type 1
R_3	Inner radius of opening slot type 2
R_4	The outer radius of the inner stator
R_5	The inner radius of the rotor
R_6	The outer radius of the rotor
R_7	The inner radius of the outer stator
R_8	The inner radius of the outer stator yoke
N	Turns number
L	Stack length
α	The angle of the ith slot within Region I
β_1	The angle of the jth slot within Region II (slot-opening type 1)
β_2	The angle of the kth slot in Region III (slot-opening type 2)
γ	The angle of the lth PM within Region V
δ	The angle of the mth slot within Region VII
P_r	Pole-pair number of rotor's permanent magnets (PMs)
P_w	Pole-pair numbers of the inner and outer stators' windings
Z	Slot numbers of the inner and outer stators
J_z	Current density

$A_{I,i}$	MVP of the *i*th slot in Region I
$A_{II,j}$	MVP of the *j*th slot within Region II
$A_{III,k}$	MVP of the *k*th slot within Region III
A_{IV}	MVP within Region IV
$A_{V,l}$	MVP of the *l*th slot within Region V
A_{VI}	MVP within Region VI
$A_{VII,m}$	MVP of the *m*th slot within Region VII
θ_i	The initial angle of the *i*th slot in Region I
θ_j	The initial angle of the *j*th slot within Region II
θ_k	The initial angle of the *k*th slot within Region III
$M_{\theta,l}$	Tangential magnetization of the *l*th PM within Region V
θ_l	The initial angle of the *l*th PM within Region V
θ_m	The initial angle of the *m*th slot within Region VII

Appendix A

By applying the method of separation of variables, the complementary solution to (2) is deducted as follows. Considering various materials' properties, the magnetic vector potential (MVP) A_z in the polar coordinates is:

$$\frac{\partial A_z}{\partial r^2} + \frac{1}{r}\frac{\partial A_z}{\partial r} + \frac{1}{r^2}\frac{\partial A_z}{\partial \theta^2} = -\frac{\mu_0}{r}\left(\frac{\partial (r \cdot M_\theta)}{\partial r} - \frac{\partial M_r}{\partial \theta}\right) - \mu_0 J_z \tag{A1}$$

The homogeneous form of (A1) is Laplace's equation:

$$\frac{\partial A_z}{\partial r^2} + \frac{1}{r}\frac{\partial A_z}{\partial r} + \frac{1}{r^2}\frac{\partial A_z}{\partial \theta^2} = 0 \tag{A2}$$

After the separation of variables, $A_z(r,\theta)$ can be written as:

$$A_z(r,\theta) = R(r)\Theta(\theta) \tag{A3}$$

After bringing (A3) back into (A2):

$$\frac{r}{R(r)}\left(\frac{r \cdot d^2R(r)}{dr^2} + \frac{dR(r)}{dr}\right) = -\frac{1}{\Theta(\theta)}\frac{d^2\Theta(\theta)}{d\theta^2} = \lambda \tag{A4}$$

According to the ordinary differential equation theory, when $\lambda = 0$, the solution of $R(r)$ and $\Theta(\theta)$ in (A4) are as follows:

$$R(r) = A_0 + B_0 \ln r,\ \Theta(\theta) = C_0\theta + D_0 \tag{A5}$$

When $\lambda = n^2$ (n is the positive integer), the solutions of $R(r)$ and $\Theta(\theta)$ in (A4) are as follows:

$$R(r) = A_n r^n + B_n r^{-n}, \Theta(\theta) = C_n \cos n\theta + D_n \sin n\theta \tag{A6}$$

When $\lambda = -n^2$ (n is the positive integer), the solutions of $R(r)$ and $\Theta(\theta)$ in (A4) are as follows:

$$R(r) = E_n \sin(n \ln r) + F_n \cos(n \ln r),\ \Theta(\theta) = G_n e^{n\theta} + H_n e^{-n\theta} \tag{A7}$$

Considering $\lambda = 0$, $\lambda = n^2$ and $\lambda = -n^2$, as well as n with different values, the complementary solution to (A1) can be written as:

$$\begin{aligned} A_z(r,\theta) &= (A_0 + B_0 \ln r)(C_0\theta + D_0) \\ &+ \sum_{n=1}^{\infty} (A_n r^n + B_n r^{-n})(C_n \cos n\theta + D_n \sin n\theta) \\ &+ \sum_{n=1}^{\infty} [E_n \sin(n \ln r) + F_n \cos(n \ln r)](G_n e^{n\theta} + H_n e^{-n\theta}) \end{aligned} \tag{A8}$$

Considering the periodic boundary condition $A_z(r,\theta)|_{\theta=0} = A_z(r,\theta)|_{\theta=2\pi}$ for $\forall r$, we obtain $C_0 = 0$, $G_n = 0$ and $H_n = 0$. After merging $(A_0 + B_0 \ln r)D_0$ as $A_0 + B_0 \ln r$, (A8) can be simplified as:

$$A_z(r,\theta) = (A_0 + B_0 \ln r) + \sum_{n=1}^{\infty} \left(A_n r^n + B_n r^{-n}\right)(C_n \cos n\theta + D_n \sin n\theta) \tag{A9}$$

Considering $A_z(r,\theta)$ is finite when $r = 0$, we then obtain $B_0 = 0$. Therefore, (A9) can be further simplified as:

$$A_z(r,\theta) = A_0 + \sum_{n=1}^{\infty} \left(A_n r^n + B_n r^{-n}\right)(C_n \cos n\theta + D_n \sin n\theta) \tag{A10}$$

Taking Region VI as an example, in Region VI, magnetic vector potential (MVP) is:

$$A_{VI}(r,\theta) = A_0^{VI} + \sum_{n=1}^{\infty} (A_{n_6}^{VI} r^{n_6} + B_{n_6}^{VI} r^{-n_6})(C_{n_6}^{VI} \cos n_6\theta + D_{n_6}^{VI} \sin n_6\theta) \tag{A11}$$

Then we can rewrite the form of $A_{VI}(r,\theta)$ with the values of $A_{n_6}^{VI}$, $B_{n_6}^{VI}$, $C_{n_6}^{VI}$ and $D_{n_6}^{VI}$ change (as $A_{n_6}^{VI}$, $B_{n_6}^{VI}$, $C_{n_6}^{VI}$ and $D_{n_6}^{VI}$ are the unknown coefficients so they can be redetermined after the expression of $A_{VI}(r,\theta)$ changes and the value of $A_{VI}(r,\theta)$ keep unchanged):

$$\begin{aligned} A_{VI}(r,\theta) &= A_0^{VI} + \sum_{n_6=1}^{\infty} \left(A_{n_6}^{VI} r^{n_6} + B_{n_6}^{VI} r^{-n_6}\right) \cdot \cos(n_6\theta) \\ &+ \sum_{n_6=1}^{\infty} \left(C_{n_6}^{VI} r^{n_6} + D_{n_6}^{VI} r^{-n_6}\right) \cdot \sin(n_6\theta) \end{aligned} \tag{A12}$$

Alternatively, the following form:

$$\begin{aligned} A_{VI}(r,\theta) &= A_0^{VI} + \sum_{n_6=1}^{\infty} \left(A_{n_6}^{VI} \left(\frac{r}{R_7}\right)^{n_6} + B_{n_6}^{VI} \left(\frac{r}{R_6}\right)^{-n_6}\right) \cdot \cos(n_6\theta) \\ &+ \sum_{n_6=1}^{\infty} \left(C_{n_6}^{VI} \left(\frac{r}{R_7}\right)^{n_6} + D_{n_6}^{VI} \left(\frac{r}{R_6}\right)^{-n_6}\right) \cdot \sin(n_6\theta) \end{aligned} \tag{A13}$$

After the mathematical deduction, we obtain the following equations (notice that $A_{n_6}^{VI}$, $B_{n_6}^{VI}$, $C_{n_6}^{VI}$ and $D_{n_6}^{VI}$ change after the deduction; however, they are the unknown coefficients so we can solve them with the proper value while $A_{VI}(r,\theta)$ keeping unchanged:

$$\begin{aligned} A_{VI}(r,\theta) = \quad & A_0^{VI} + \sum_{n_6=1}^{\infty} \left(\frac{\left(A_{n_6}^{VI} \frac{R_6}{n_6} \left(\frac{1}{R_7}\right)^{n_6} - B_{n_6}^{VI} \frac{R_7}{n_6} \left(\frac{1}{R_6}\right)^{n_6}\right)}{\left(\frac{R_6}{R_7}\right)^{n_6} - \left(\frac{R_7}{R_6}\right)^{n_6}} r^{n_6} + \frac{\left(A_{n_6}^{VI} \frac{R_6}{n_6} \left(\frac{R_7}{1}\right)^{n_6} - B_{n_6}^{VI} \frac{R_7}{n_6} \left(\frac{R_6}{1}\right)^{n_6}\right)}{\left(\frac{R_6}{R_7}\right)^{n_6} - \left(\frac{R_7}{R_6}\right)^{n_6}} r^{-n_6} \right) \cdot \cos(n_6\theta) \\ & + \sum_{n_6=1}^{\infty} \left(\frac{\left(C_{n_6}^{VI} \frac{R_6}{n_6} \left(\frac{1}{R_7}\right)^{n_6} - D_{n_6}^{VI} \frac{R_7}{n_6} \left(\frac{1}{R_6}\right)^{n_6}\right)}{\left(\frac{R_6}{R_7}\right)^{n_6} - \left(\frac{R_7}{R_6}\right)^{n_6}} r^{n_6} + \frac{\left(C_{n_6}^{VI} \frac{R_6}{n_6} \left(\frac{R_7}{1}\right)^{n_6} - D_{n_6}^{VI} \frac{R_7}{n_6} \left(\frac{R_6}{1}\right)^{n_6}\right)}{\left(\frac{R_6}{R_7}\right)^{n_6} - \left(\frac{R_7}{R_6}\right)^{n_6}} r^{-n_6} \right) \cdot \sin(n_6\theta) \end{aligned} \tag{A14}$$

Therefore, we get:

$$\begin{aligned} A_{VI}(r,\theta) = A_0^{VI} \quad & + \sum_{n_6=1}^{\infty} \begin{pmatrix} A_{n_6}^{VI} \frac{R_6}{n_6} \left(\frac{1}{R_7}\right)^{n_6} \frac{r^{n_6}}{\left(\frac{R_6}{R_7}\right)^{n_6} - \left(\frac{R_7}{R_6}\right)^{n_6}} - B_{n_6}^{VI} \frac{R_7}{n_6} \left(\frac{1}{R_6}\right)^{n_6} \frac{r^{n_6}}{\left(\frac{R_6}{R_7}\right)^{n_6} - \left(\frac{R_7}{R_6}\right)^{n_6}} \\ + A_{n_6}^{VI} \frac{R_6}{n_6} R_7{}^{n_6} \frac{r^{-n_6}}{\left(\frac{R_6}{R_7}\right)^{n_6} - \left(\frac{R_7}{R_6}\right)^{n_6}} - B_{n_6}^{VI} \frac{R_7}{n_6} R_6{}^{n_6} \frac{r^{-n_6}}{\left(\frac{R_6}{R_7}\right)^{n_6} - \left(\frac{R_7}{R_6}\right)^{n_6}} \end{pmatrix} \cdot \cos(n_6\theta) \\ & + \sum_{n_6=1}^{\infty} \begin{pmatrix} C_{n_6}^{VI} \frac{R_6}{n_6} \left(\frac{1}{R_7}\right)^{n_6} \frac{r^{n_6}}{\left(\frac{R_6}{R_7}\right)^{n_6} - \left(\frac{R_7}{R_6}\right)^{n_6}} - D_{n_6}^{VI} \frac{R_7}{n_6} \left(\frac{1}{R_6}\right)^{n_6} \frac{r^{n_6}}{\left(\frac{R_6}{R_7}\right)^{n_6} - \left(\frac{R_7}{R_6}\right)^{n_6}} \\ + C_{n_6}^{VI} \frac{R_6}{n_6} R_7{}^{n_6} \frac{r^{-n_6}}{\left(\frac{R_6}{R_7}\right)^{n_6} - \left(\frac{R_7}{R_6}\right)^{n_6}} - D_{n_6}^{VI} \frac{R_7}{n_6} R_6{}^{n_6} \frac{r^{-n_6}}{\left(\frac{R_6}{R_7}\right)^{n_6} - \left(\frac{R_7}{R_6}\right)^{n_6}} \end{pmatrix} \cdot \sin(n_6\theta) \end{aligned} \tag{A15}$$

Consequently,

$$A_{VI}(r,\theta) = A_0^{VI} + \sum_{n_6=1}^{\infty}\left(\begin{array}{l} A_{n_6}^{VI}\frac{R_6}{n_6}\frac{\left(\frac{r}{R_7}\right)^{n_6}}{\left(\frac{R_6}{R_7}\right)^{n_6}-\left(\frac{R_7}{R_6}\right)^{n_6}} + A_{n_6}^{VI}\frac{R_6}{n_6}\frac{\left(\frac{R_7}{r}\right)^{n_6}}{\left(\frac{R_6}{R_7}\right)^{n_6}-\left(\frac{R_7}{R_6}\right)^{n_6}} \\ -B_{n_6}^{VI}\frac{R_7}{n_6}\frac{\left(\frac{r}{R_6}\right)^{n_6}}{\left(\frac{R_6}{R_7}\right)^{n_6}-\left(\frac{R_7}{R_6}\right)^{n_6}} - B_{n_6}^{VI}\frac{R_7}{n_6}\frac{\left(\frac{R_6}{r}\right)^{n_6}}{\left(\frac{R_6}{R_7}\right)^{n_6}-\left(\frac{R_7}{R_6}\right)^{n_6}} \end{array}\right)\cdot\cos(n_6\theta) + \sum_{n_6=1}^{\infty}\left(\begin{array}{l} C_{n_6}^{VI}\frac{R_6}{n_6}\frac{\left(\frac{r}{R_7}\right)^{n_6}}{\left(\frac{R_6}{R_7}\right)^{n_6}-\left(\frac{R_7}{R_6}\right)^{n_6}} + C_{n_6}^{VI}\frac{R_6}{n_6}\frac{\left(\frac{R_7}{r}\right)^{n_6}}{\left(\frac{R_6}{R_7}\right)^{n_6}-\left(\frac{R_7}{R_6}\right)^{n_6}} \\ -D_{n_6}^{VI}\frac{R_7}{n_6}\frac{\left(\frac{r}{R_6}\right)^{n_6}}{\left(\frac{R_6}{R_7}\right)^{n_6}-\left(\frac{R_7}{R_6}\right)^{n_6}} - D_{n_6}^{VI}\frac{R_7}{n_6}\frac{\left(\frac{R_6}{r}\right)^{n_6}}{\left(\frac{R_6}{R_7}\right)^{n_6}-\left(\frac{R_7}{R_6}\right)^{n_6}} \end{array}\right)\cdot\sin(n_6\theta) \tag{A16}$$

After a similar terms' combination, we get:

$$A_{VI}(r,\theta) = A_0^{VI} + \sum_{n_6=1}^{\infty}\left(A_{n_6}^{VI}\frac{R_6}{n_6}\frac{\left(\frac{r}{R_7}\right)^{n_6}+\left(\frac{R_7}{r}\right)^{n_6}}{\left(\frac{R_6}{R_7}\right)^{n_6}-\left(\frac{R_7}{R_6}\right)^{n_6}} + B_{n_6}^{VI}\frac{R_7}{n_6}\frac{\left(\frac{r}{R_6}\right)^{n_6}+\left(\frac{R_6}{r}\right)^{n_6}}{\left(\frac{R_7}{R_6}\right)^{n_6}-\left(\frac{R_6}{R_7}\right)^{n_6}}\right)\cdot\cos(n_6\theta) + \sum_{n_6=1}^{\infty}\left(C_{n_6}^{VI}\frac{R_6}{n_6}\frac{\left(\frac{r}{R_7}\right)^{n_6}+\left(\frac{R_7}{r}\right)^{n_6}}{\left(\frac{R_6}{R_7}\right)^{n_6}-\left(\frac{R_7}{R_6}\right)^{n_6}} + D_{n_6}^{VI}\frac{R_7}{n_6}\frac{\left(\frac{r}{R_6}\right)^{n_6}+\left(\frac{R_6}{r}\right)^{n_6}}{\left(\frac{R_7}{R_6}\right)^{n_6}-\left(\frac{R_6}{R_7}\right)^{n_6}}\right)\cdot\sin(n_6\theta) \tag{A17}$$

The relationship between $P_w(u,v)$ and $E_w(u,v)$ is listed for further simplification:

$$P_w(u,v) = \left(\frac{u}{v}\right)^w + \left(\frac{v}{u}\right)^w, E_w(u,v) = \left(\frac{u}{v}\right)^w - \left(\frac{v}{u}\right)^w \tag{A18}$$

$$\frac{\partial P_w(u,v)}{\partial u} = E_w(u,v), \frac{\partial E_w(u,v)}{\partial u} = P_w(u,v) \tag{A19}$$

Because of the relationship between $P_w(u,v)$ and $E_w(u,v)$, it is easy to obtain the derivative in complicated expressions when the expression needs the derivative (when utilizing the boundary conditions), therefore, we obtain the form of $A_{VI}(r,\theta)$, containing $P_w(u,v)$ and $E_w(u,v)$ for simplification:

$$A_{VI}(r,\theta) = A_0^{VI} + \sum_{n_6=1}^{\infty}\left(A_{n_6}^{VI}\frac{R_6}{n_6}\frac{P_{n_6}(r,R_7)}{E_{n_6}(R_6,R_7)} + B_{n_6}^{VI}\frac{R_7}{n_6}\frac{P_{n_6}(r,R_6)}{E_{n_6}(R_7,R_6)}\right)\cdot\cos(n_6\theta) + \sum_{n_6=1}^{\infty}\left(C_{n_6}^{VI}\frac{R_6}{n_6}\frac{P_{n_6}(r,R_7)}{E_{n_6}(R_6,R_7)} + D_{n_6}^{VI}\frac{R_7}{n_6}\frac{P_{n_6}(r,R_6)}{E_{n_6}(R_7,R_6)}\right)\cdot\sin(n_6\theta) \tag{A20}$$

After utilizing boundary conditions (33) and (34), we get:

$$\left.\frac{\partial A_{VI}}{\partial r}\right|_{r=R_6} = \sum_{n_6=1}^{\infty}\left(A_{n_6}^{VI}\frac{R_6}{n_6}\frac{E_{n_6}(R_6,R_7)}{E_{n_6}(R_6,R_7)} + B_{n_6}^{VI}\frac{R_7}{n_6}\frac{E_{n_6}(R_6,R_6)}{E_{n_6}(R_7,R_6)}\right)\cdot\cos(n_6\theta) + \sum_{n_6=1}^{\infty}\left(C_{n_6}^{VI}\frac{R_6}{n_6}\frac{E_{n_6}(R_6,R_7)}{E_{n_6}(R_6,R_7)} + D_{n_6}^{VI}\frac{R_7}{n_6}\frac{E_{n_6}(R_6,R_6)}{E_{n_6}(R_7,R_6)}\right)\cdot\sin(n_6\theta) = g_1(\theta) \tag{A21}$$

According to:

$$P_w(u,u) = \left(\frac{u}{u}\right)^w + \left(\frac{u}{u}\right)^w = 2 \tag{A22}$$

$$E_w(u,u) = \left(\frac{u}{u}\right)^w - \left(\frac{u}{u}\right)^w = 0 \tag{A23}$$

$$\frac{E_{n_6}(R_6,R_7)}{E_{n_6}(R_6,R_7)} = 1, E_{n_6}(R_6,R_6) = 0 \tag{A24}$$

Therefore, we get:

$$\left.\frac{\partial A_{VI}}{\partial r}\right|_{r=R_6} = \sum_{n_6=1}^{\infty}\left(A_{n_6}^{VI}\frac{R_6}{n_6}\right)\cdot\cos(n_6\theta) + \sum_{n_6=1}^{\infty}\left(C_{n_6}^{VI}\frac{R_6}{n_6}\right)\cdot\sin(n_6\theta) = g_1(\theta) \tag{A25}$$

Similarly, according to:

$$\frac{E_{n_6}(R_7,R_6)}{E_{n_6}(R_7,R_6)}=1, E_{n_6}(R_7,R_7)=0 \tag{A26}$$

Then we get:

$$\left.\frac{\partial A_{VI}}{\partial r}\right|_{r=R_7}=\sum_{n_6=1}^{\infty}\left(B_{n_6}^{VI}\frac{R_7}{n_6}\right)\cdot\cos(n_6\theta)+\sum_{n_6=1}^{\infty}\left(D_{n_6}^{VI}\frac{R_7}{n_6}\right)\cdot\sin(n_6\theta)=g_2(\theta) \tag{A27}$$

According to a generalized Fourier series expansion of (A25) and (A27), we obtain the following equations:

$$A_{n_6}^{VI}=\frac{1}{\pi}\int_0^{2\pi}\left.\frac{\partial A_{VI}}{\partial r}\right|_{r=R_6}\cos(n_6\theta)d\theta\ ;\quad C_{n_6}^{VI}=\frac{1}{\pi}\int_0^{2\pi}\left.\frac{\partial A_{VI}}{\partial r}\right|_{r=R_6}\sin(n_6\theta)d\theta \tag{A28}$$

$$B_{n_6}^{VI}=\frac{1}{\pi}\int_0^{2\pi}\left.\frac{\partial A_{VI}}{\partial r}\right|_{r=R_7}\cos(n_6\theta)d\theta\ ;\quad D_{n_6}^{VI}=\frac{1}{\pi}\int_0^{2\pi}\left.\frac{\partial A_{VI}}{\partial r}\right|_{r=R_7}\sin(n_6\theta)d\theta \tag{A29}$$

Finally, after simplification, we obtain the following equations:

$$A_{n_6}^{VI}=\frac{1}{\pi}\int_0^{2\pi}g_1(\theta)\cos(n_6\theta)d\theta\ ;\ C_{n_6}^{VI}=\frac{1}{\pi}\int_0^{2\pi}g_1(\theta)\sin(n_6\theta)d\theta \tag{A30}$$

$$B_{n_6}^{VI}=\frac{1}{\pi}\int_0^{2\pi}g_2(\theta)\cos(n_6\theta)d\theta\ ;\ D_{n_6}^{VI}=\frac{1}{\pi}\int_0^{2\pi}g_2(\theta)\sin(n_6\theta)d\theta \tag{A31}$$

Appendix B

The unknown Fourier series coefficients in the MVP expression of each subdomain need to be deduced and calculated for consequent Fourier series coefficient matrices solution. The detailed Fourier series coefficients in the MVP expression of each subdomain can be calculated via the Fourier expansion in each subdomain boundary and applying the adjacent subdomain MVP values or derivative information. Therefore, the detailed Fourier series coefficients in each subdomain of DSVMs can be calculated as follows.

First of all, according to the definition of (4) and (5), the relationship between $P_w(u,v)$ and $E_w(u,v)$ is described as follows for later clarity and simplicity in the partial derivation:

$$\frac{\partial P_w(u,v)}{\partial u}=E_w(u,v) \tag{A32}$$

$$\frac{\partial E_w(u,v)}{\partial u}=P_w(u,v) \tag{A33}$$

In Region I, considering the boundary condition of Region I and Region II, after substituting (12) into (9), we get:

$$\begin{aligned}A_{n_1}^i &= \tfrac{4B_0^j}{n_1\pi R_2}\sin(\tfrac{n_1\pi\beta_1}{2\alpha})\cos(\tfrac{n_1\pi}{2})\\ &+\sum_{n_2=1}^{\infty}(A_{n_2}^j\tfrac{P_{n_2\pi/\beta_1}(R_2,R_4)}{E_{n_2\pi/\beta_1}(R_2,R_4)}-B_{n_2}^j\tfrac{2}{E_{n_2\pi/\beta_1}(R_2,R_4)})\cdot\tfrac{2n_2\pi}{\alpha\beta_1R_2}\cdot F(n_1,n_2)\end{aligned} \tag{A34}$$

In Region II, considering the boundary condition of Region I and Region II, after substituting (8) into (15), considering the boundary condition of Region II and Region IV, after substituting (23) into (16), we get:

$$\begin{aligned} A_{n_2}^{j} = & \sum_{n_1=1}^{\infty} \Big(A_{n_1}^{i} \tfrac{2\alpha R_2}{n_1\pi\beta_1} \tfrac{P_{n_1\pi/\alpha}(R_2,R_1)}{E_{n_1\pi/\alpha}(R_2,R_1)} \\ & - \tfrac{2\mu_0 J_{in}}{\beta_1\left((n_1\pi/\alpha)^2-4\right)} \big(\tfrac{2\alpha}{n_1\pi} \tfrac{R_1^2\cdot 2-R_2^2 P_{n_1\pi/\alpha}(R_2,R_1)}{E_{n_1\pi/\alpha}(R_2,R_1)} + R_2^2\big) \cdot F(n_1,n_2) \end{aligned} \tag{A35}$$

$$\begin{aligned} B_{n_2}^{j} = & \sum_{n_4=1}^{\infty} \big(A_{n_4}^{IV} \tfrac{2R_4}{n_4\beta_1} \tfrac{P_{n_4}(R_4,R_5)}{E_{n_4}(R_4,R_5)} + B_{n_4}^{IV} \tfrac{2R_5}{n_4\beta_1} \tfrac{2}{E_{n_4}(R_5,R_4)}\big) \cdot f_a(n_2,n_4,j) \\ & + \sum_{n_4=1}^{\infty} \big(C_{n_4}^{IV} \tfrac{2R_4}{n_4\beta_1} \tfrac{P_{n_4}(R_4,R_5)}{E_{n_4}(R_4,R_5)} + D_{n_4}^{IV} \tfrac{2R_5}{n_4\beta_1} \tfrac{2}{E_{n_4}(R_5,R_4)}\big) \cdot g_a(n_2,n_4,j) \end{aligned} \tag{A36}$$

In Region III, considering the boundary condition of Region III and Region IV, after substituting (23) into (20), we get:

$$\begin{aligned} A_{n_3}^{k} = & \sum_{n_4=1}^{\infty} \big(A_{n_4}^{IV} \tfrac{2R_4}{n_4\beta_1} \tfrac{P_{n_4}(R_4,R_5)}{E_{n_4}(R_4,R_5)} + B_{n}^{IV} \tfrac{2R_5}{n_4\beta_1} \tfrac{2}{E_{n_4}(R_5,R_4)}\big) \cdot f_t(n_3,n_4,k) \\ & + \sum_{n_4=1}^{\infty} \big(A_{n_4}^{IV} \tfrac{2R_4}{n_4\beta_1} \tfrac{P_{n_4}(R_4,R_5)}{E_{n_4}(R_4,R_5)} + B_{n}^{IV} \tfrac{2R_5}{n_4\beta_1} \tfrac{2}{E_{n_4}(R_5,R_4)}\big) \cdot g_t(n_3,n_4,k) \end{aligned} \tag{A37}$$

In Region IV, considering the boundary condition of Region IV, Region II, and Region III, after substituting (12), (19) and (21) into (24), considering the boundary condition of Region IV and Region V, after substituting (22) and (28) into (25), we get:

$$\begin{aligned} A_{n_4}^{IV} = & \sum_{j=1}^{P_i} \tfrac{B_0^j}{\pi R_4} \cdot r_j(n_4,j) + \sum_{j=1}^{P_i} \sum_{n_2=1}^{\infty} A_{n_2}^{j} \tfrac{n_2}{\beta_1 R_4} \tfrac{2}{E_{n_2\pi/\beta_1}(R_2,R_4)} \cdot f_a(n_2,n_4,j) \\ & - \sum_{j=1}^{P_i} \sum_{n_2=1}^{\infty} B_{n_2}^{j} \tfrac{n_2}{\beta_1 R_4} \tfrac{P_{n_2\pi/\beta_1}(R_4,R_2)}{E_{n_2\pi/\beta_1}(R_2,R_4)} \cdot f_a(n_2,n_4,j) \\ & + \sum_{k=1}^{P_i} \sum_{n_3=1}^{\infty} A_{n_3}^{k} \tfrac{n_3}{\beta_2 R_4} \tfrac{E_{n_3\pi/\beta_2}(R_4,R_3)}{P_{n_3\pi/\beta_2}(R_3,R_4)} \cdot f_t(n_3,n_4,k) \end{aligned} \tag{A38}$$

$$\begin{aligned} C_{n_4}^{IV} = & \sum_{j=1}^{P_i} \tfrac{B_0^j}{\pi R_4} \cdot s_j(n_4,j) + \sum_{j=1}^{P_i} \sum_{n_2=1}^{\infty} A_{n_2}^{j} \tfrac{n_2}{\beta_1 R_4} \tfrac{2}{E_{n_2\pi/\beta_1}(R_2,R_4)} \cdot g_a(n_2,n_4,j) \\ & - \sum_{j=1}^{P_i} \sum_{n_2=1}^{\infty} B_{n_2}^{j} \tfrac{n_2}{\beta_1 R_4} \tfrac{P_{n_2\pi/\beta_1}(R_4,R_2)}{E_{n_2\pi/\beta_1}(R_2,R_4)} \cdot g_a(n_2,n_4,j) \\ & + \sum_{k=1}^{P_i} \sum_{n_3=1}^{\infty} A_{n_3}^{k} \tfrac{n_3}{\beta_2 R_4} \tfrac{E_{n_3\pi/\beta_2}(R_4,R_3)}{P_{n_3\pi/\beta_2}(R_3,R_4)} \cdot g_t(n_3,n_4,k) \end{aligned} \tag{A39}$$

$$\begin{aligned} B_{n_4}^{IV} = & \sum_{l=1}^{Q} \tfrac{B_0^l}{\pi R_5} \cdot r_f(n_4,l) + \sum_{l=1}^{Q} \sum_{n_5=1}^{\infty} A_{n_5}^{l} \tfrac{n_5}{\gamma R_5} \tfrac{P_{n_5\pi/\gamma}(R_5,R_6)}{E_{n_5\pi/\gamma}(R_5,R_6)} \cdot f_f(n_5,n_4,l) \\ & - \sum_{l=1}^{Q} \sum_{n_5=1}^{\infty} B_{n_5}^{l} \tfrac{n_5}{\gamma R_5} \tfrac{2}{E_{n_5\pi/\gamma}(R_5,R_6)} \cdot f_f(n_5,n_4,l) \end{aligned} \tag{A40}$$

$$\begin{aligned} D_{n_4}^{IV} = & \sum_{l=1}^{Q} \tfrac{B_0^l}{\pi R_5} \cdot s_f(n_4,l) + \sum_{l=1}^{Q} \sum_{n_5=1}^{\infty} A_{n_5}^{l} \tfrac{n_5}{\gamma R_5} \tfrac{P_{n_5\pi/\gamma}(R_5,R_6)}{E_{n_5\pi/\gamma}(R_5,R_6)} \cdot g_f(n_5,n_4,l) \\ & - \sum_{l=1}^{Q} \sum_{n_5=1}^{\infty} B_{n_5}^{l} \tfrac{n_5}{\gamma R_5} \tfrac{2}{E_{n_5\pi/\gamma}(R_5,R_6)} \cdot g_f(n_5,n_4,l) \end{aligned} \tag{A41}$$

In Region V, considering the boundary condition of Region V and Region IV, after substituting (23) into (29) and (31), considering the boundary condition of Region V and Region VI, after substituting (35) into (30) and (32), we get:

$$\begin{aligned} A_{n_5}^{l} &= \sum_{n_4=1}^{\infty}\left(A_{n_4}^{IV}\frac{2R_4}{n_4\gamma}\frac{2}{E_{n_4}(R_4,R_5)} + B_{n_4}^{IV}\frac{2R_5}{n_4\gamma}\frac{P_{n_4}(R_5,R_4)}{E_{n_4}(R_5,R_4)}\right)\cdot f_f(n_5,n_4,l) \\ &+ \sum_{n_4=1}^{\infty}\left(C_{n_4}^{IV}\frac{2R_4}{n_4\gamma}\frac{2}{E_{n_4}(R_4,R_5)} + D_{n_4}^{IV}\frac{2R_5}{n_4\gamma}\frac{P_{n_4}(R_5,R_4)}{E_{n_4}(R_5,R_4)}\right)\cdot g_f(n_5,n_4,l) \end{aligned} \tag{A42}$$

$$\begin{aligned} B_{n_5}^{l} &= \sum_{n_6=1}^{\infty}\left(A_{n_6}^{VI}\frac{2R_6}{n_6\gamma}\frac{P_{n_6}(R_6,R_7)}{E_{n_6}(R_6,R_7)} + B_{n_6}^{VI}\frac{2R_7}{n_6\gamma}\frac{2}{E_{n_6}(R_7,R_6)}\right)\cdot f_f(n_5,n_6,l) \\ &+ \sum_{n_6=1}^{\infty}\left(C_{n_6}^{VI}\frac{2R_6}{n_6\gamma}\frac{P_{n_6}(R_6,R_7)}{E_{n_6}(R_6,R_7)} + D_{n_6}^{VI}\frac{2R_7}{n_6\gamma}\frac{2}{E_{n_6}(R_7,R_6)}\right)\cdot g_f(n_5,n_6,l) \end{aligned} \tag{A43}$$

$$\begin{aligned} A_0^{l} &+ B_0^{l}\ln R_5 - \mu_0 M_{\theta,l}R_5 = \\ A_0^{IV} &+ \sum_{n_4=1}^{\infty}\left(A_{n_4}^{IV}\frac{R_4}{n_4\gamma}\frac{2}{E_{n_4}(R_4,R_5)} + B_{n_4}^{IV}\frac{R_5}{n_4\gamma}\frac{P_{n_4}(R_5,R_4)}{E_{n_4}(R_5,R_4)}\right)\cdot r_f(n_4,l) \\ &+ \sum_{n_4=1}^{\infty}\left(C_{n_4}^{IV}\frac{R_4}{n_4\gamma}\frac{2}{E_{n_4}(R_4,R_5)} + D_{n_4}^{IV}\frac{R_5}{n_4\gamma}\frac{P_{n_4}(R_5,R_4)}{E_{n_4}(R_5,R_4)}\right)\cdot s_f(n_4,l) \end{aligned} \tag{A44}$$

$$\begin{aligned} A_0^{l} &+ B_0^{l}\ln R_6 - \mu_0 M_{\theta,l}R_6 = \\ A_0^{VI} &+ \sum_{n_6=1}^{\infty}\left(A_{n_6}^{VI}\frac{R_6}{n_6\gamma}\frac{P_{n_6}(R_6,R_7)}{E_{n_6}(R_6,R_7)} + B_{n_6}^{VI}\frac{R_7}{n_6\gamma}\frac{2}{E_{n_6}(R_7,R_6)}\right)\cdot r_f(n_6,l) \\ &+ \sum_{n_6=1}^{\infty}\left(C_{n_6}^{VI}\frac{R_6}{n_6\gamma}\frac{P_{n_6}(R_6,R_7)}{E_{n_6}(R_6,R_7)} + D_{n_6}^{VI}\frac{R_7}{n_6\gamma}\frac{2}{E_{n_6}(R_7,R_6)}\right)\cdot s_f(n_6,l) \end{aligned} \tag{A45}$$

In Region VI, considering the boundary condition of Region VI and Region V, after substituting (28) and (33) into (36), considering the boundary condition of Region VI and Region VII, after substituting (34) and (40) into (37), we get:

$$\begin{aligned} A_{n_6}^{VI} &= \sum_{l=1}^{Q}\frac{B_0^l}{\pi R_6}\cdot r_f(n_6,l) + \sum_{l=1}^{Q}\sum_{n_5=1}^{\infty}A_{n_5}^{l}\frac{n_5}{\gamma R_6}\frac{2}{E_{n_5\pi/\gamma}(R_5,R_6)}\cdot f_f(n_5,n_6,l) \\ &-\sum_{l=1}^{Q}\sum_{n_5=1}^{\infty}B_{n_5}^{l}\frac{n_5}{\gamma R_6}\frac{P_{n_5\pi/\gamma}(R_6,R_5)}{E_{n_5\pi/\gamma}(R_5,R_6)}\cdot f_f(n_5,n_6,l) \end{aligned} \tag{A46}$$

$$\begin{aligned} C_{n_6}^{VI} &= \sum_{l=1}^{Q}\frac{B_0^l}{\pi R_6}\cdot s_f(n_6,l) + \sum_{l=1}^{Q}\sum_{n_5=1}^{\infty}A_{n_5}^{l}\frac{n_5}{\gamma R_6}\frac{2}{E_{n_5\pi/\gamma}(R_5,R_6)}\cdot g_f(n_5,n_6,l) \\ &-\sum_{l=1}^{Q}\sum_{n_5=1}^{\infty}B_{n_5}^{l}\frac{n_5}{\gamma R_6}\frac{P_{n_5\pi/\gamma}(R_6,R_5)}{E_{n_5\pi/\gamma}(R_5,R_6)}\cdot g_f(n_5,n_6,l) \end{aligned} \tag{A47}$$

$$\begin{aligned} B_{n_6}^{VI} &= \sum_{m=1}^{P_o}\frac{\mu_0 J_m}{2\pi}\left(\frac{R_8^2}{R_7} - R_7\right)\cdot r_s(n_6,m) \\ &+ \sum_{m=1}^{P_o}\sum_{n_7=1}^{\infty}A_{n_7}^{m}\frac{n_7}{\delta R_7}\frac{E_{n_7\pi/\delta}(R_7,R_8)}{P_{n_7\pi/\delta}(R_7,R_8)}\cdot f_s(n_7,n_6,m) \end{aligned} \tag{A48}$$

$$\begin{aligned} D_{n_6}^{VI} &= \sum_{m=1}^{P_o}\frac{\mu_0 J_m}{2\pi}\left(\frac{R_8^2}{R_7} - R_7\right)\cdot s_s(n_6,m) \\ &+ \sum_{m=1}^{P_o}\sum_{n_7=1}^{\infty}A_{n_7}^{m}\frac{n_7}{\delta R_7}\frac{E_{n_7\pi/\delta}(R_7,R_8)}{P_{n_7\pi/\delta}(R_7,R_8)}\cdot g_s(n_7,n_6,m) \end{aligned} \tag{A49}$$

In Region VII, considering the boundary condition of Region VI and Region VII, after substituting (35) into (41), we get:

$$\begin{aligned} A_{n_7}^{m} &= \sum_{n_6=1}^{\infty}\left(A_{n_6}^{VI}\frac{2R_6}{n_6\delta}\frac{2}{E_n(R_6,R_7)} + B_{n_6}^{VI}\frac{2R_7}{n_6\delta}\frac{P_n(R_7,R_6)}{E_n(R_7,R_6)}\right)f_s(n_7,n_6,m) \\ &+ \sum_{n_6=1}^{\infty}\left(C_{n_6}^{VI}\frac{2R_6}{n_6\delta}\frac{2}{E_n(R_6,R_7)} + D_{n_6}^{VI}\frac{2R_7}{n_6\delta}\frac{P_n(R_7,R_6)}{E_n(R_7,R_6)}\right)g_s(n_7,n_6,m) \end{aligned} \tag{A50}$$

Appendix C

The integral functions $f_a(n_2,n_4,j)$, $g_a(n_2,n_4,j)$, $f_t(n_3,n_4,k)$, $g_t(n_3,n_4,k)$, $f_f(n_5,n_4,l)$, $g_f(n_5,n_4,l)$, $f_f(n_5,n_6,l)$, $g_f(n_5,n_6,l)$, $f_s(n_7,n_6,m)$, $g_s(n_7,n_6,m)$, $r_j(n_4,j)$, $s_j(n_4,j)$, $r_f(n_4,l)$, $s_f(n_4,l)$, $r_s(n_6,m)$, $s_s(n_6,m)$ and $F(n_1,n_2)$ are expressed as follows for consequent Fourier series coefficients matrices solution:

$$f_a(n_2,n_4,j) = \int_{\theta_j}^{\theta_j+\beta_1} \cos(n_4\theta)\cos\left(\frac{n_2\pi}{\beta_1}(\theta-\theta_j)\right)d\theta \tag{A51}$$

$$g_a(n_2,n_4,j) = \int_{\theta_j}^{\theta_j+\beta_1} \sin(n_4\theta)\cos\left(\frac{n_2\pi}{\beta_1}(\theta-\theta_j)\right)d\theta \tag{A52}$$

$$f_t(n_3,n_4,k) = \int_{\theta_k}^{\theta_k+\beta_2} \cos(n_4\theta)\cos\left(\frac{n_3\pi}{\beta_2}(\theta-\theta_k)\right)d\theta \tag{A53}$$

$$g_t(n_3,n_4,k) = \int_{\theta_k}^{\theta_k+\beta_2} \sin(n_4\theta)\cos\left(\frac{n_3\pi}{\beta_2}(\theta-\theta_k)\right)d\theta \tag{A54}$$

$$f_f(n_5,n_4,l) = \int_{\theta_l}^{\theta_l+\gamma} \cos(n_4\theta)\cos\left(\frac{n_5\pi}{\gamma}(\theta-\theta_l)\right)d\theta \tag{A55}$$

$$g_f(n_5,n_4,l) = \int_{\theta_l}^{\theta_l+\gamma} \sin(n_4\theta)\cos\left(\frac{n_5\pi}{\gamma}(\theta-\theta_l)\right)d\theta \tag{A56}$$

$$f_f(n_5,n_6,l) = \int_{\theta_l}^{\theta_l+\gamma} \cos(n_6\theta)\cos\left(\frac{n_5\pi}{\gamma}(\theta-\theta_l)\right)d\theta \tag{A57}$$

$$g_f(n_5,n_6,l) = \int_{\theta_l}^{\theta_l+\gamma} \sin(n_6\theta)\cos\left(\frac{n_5\pi}{\gamma}(\theta-\theta_l)\right)d\theta \tag{A58}$$

$$f_s(n_7,n_6,m) = \int_{\theta_m}^{\theta_m+\delta} \cos(n_6\theta)\cos\left(\frac{n_7\pi}{\delta}(\theta-\theta_m)\right)d\theta \tag{A59}$$

$$g_s(n_7,n_6,m) = \int_{\theta_m}^{\theta_m+\delta} \sin(n_6\theta)\cos\left(\frac{n_7\pi}{\delta}(\theta-\theta_m)\right)d\theta \tag{A60}$$

$$r_j(n_4,j) = \int_{\theta_j}^{\theta_j+\beta_1} \cos(n_4\theta)d\theta = \frac{1}{n}\left[\sin\left(n_4(\theta_j+\beta_1)\right) - \sin(n_4\theta_j)\right] \tag{A61}$$

$$s_j(n_4,j) = \int_{\theta_j}^{\theta_j+\beta_1} \sin(n_4\theta)d\theta = \frac{1}{n}\left[-\cos\left(n_4(\theta_j+\beta_1)\right) + \cos(n_4\theta_j)\right] \tag{A62}$$

$$r_f(n_4,l) = \int_{\theta_l}^{\theta_l+\gamma} \cos(n_4\theta)d\theta = \frac{1}{n}[\sin(n_4(\theta_l+\gamma)) - \sin(n_4\theta_l)] \tag{A63}$$

$$s_f(n_4,l) = \int_{\theta_l}^{\theta_l+\gamma} \sin(n_4\theta)d\theta = \frac{1}{n}[-\cos(n_4(\theta_l+\gamma)) + \cos(n_4\theta_l)] \tag{A64}$$

$$r_f(n_6,l) = \int_{\theta_l}^{\theta_l+\gamma} \cos(n_6\theta)d\theta = \frac{1}{n}[\sin(n_6(\theta_l+\gamma)) - \sin(n_6\theta_l)] \tag{A65}$$

$$s_f(n_6,l) = \int_{\theta_l}^{\theta_l+\gamma} \sin(n_6\theta)d\theta = \frac{1}{n}[-\cos(n_6(\theta_l+\gamma)) + \cos(n_6\theta_l)] \tag{A66}$$

$$r_s(n_6,m) = \int_{\theta_m}^{\theta_m+\delta} \cos(n_6\theta)d\theta = \frac{1}{n}[\sin(n_6(\theta_m+\delta)) - \sin(n_6\theta_m)] \tag{A67}$$

$$s_s(n_6,m) = \int_{\theta_m}^{\theta_m+\delta} \sin(n_6\theta)d\theta = \frac{1}{n}[-\cos(n_6(\theta_m+\delta)) + \cos(n_6\theta_m)] \tag{A68}$$

$$F(n_1,n_2) = \int_{\theta_j}^{\theta_j+\beta_1} \cos\left(\frac{n_1\pi}{\alpha}(\theta-\theta_i)\right)\cos\left(\frac{n_2\pi}{\beta_1}(\theta-\theta_j)\right)d\theta \tag{A69}$$

Then, $f_a(n_2, n_4, j)$, $g_a(n_2, n_4, j)$, $f_t(n_3, n_4, k)$, $g_t(n_3, n_4, k)$, $f_f(n_5, n_4, l)$, $g_f(n_5, n_4, l)$, $f_s(n_7, n_6, m)$ and $g_s(n_7, n_6, m)$ can be further simplified as:

$$f_a(n_2, n_4, j) = \begin{cases} \frac{n_4^2 {\beta_1}^2 \left[\sin(n_4\theta_j) + (-1)^{n_2+1} \sin\left(n_4(\theta_j+\beta_1)\right)\right]}{n_2^2\pi^2 - n_4^2{\beta_1}^2}, n_2\pi \neq n_4\beta_1 \\ \frac{2n_4\beta_1 \cos(n_4\theta_j) - \sin(n_4\theta_j) + \sin\left(n_4(\theta_j+\beta_1)\right)}{4n_4}, \ n_2\pi = n_4\beta_1 \end{cases} \tag{A70}$$

$$g_a(n_2, n_4, j) = \begin{cases} \frac{n_4^2 {\beta_1}^2 \left[-\cos(n_4\theta_j) + (-1)^{n_2} \cos\left(n_4(\theta_j+\beta_1)\right)\right]}{n_2^2\pi^2 - n_4^2{\beta_1}^2}, n_2\pi \neq n_4\beta_1 \\ \frac{2n_4\beta_1 \sin(n_4\theta_j) + \cos(n_4\theta_j) - \cos\left(n_4(\theta_j+\beta_1)\right)}{4n_4}, \ n_2\pi = n_4\beta_1 \end{cases} \tag{A71}$$

$$f_t(n_3, n_4, k) = \begin{cases} \frac{n_4^2 {\beta_1}^2 \left[\sin(n_4\theta_k) + (-1)^{n_3+1} \sin(n_4(\theta_k+\beta_2))\right]}{n_3^2\pi^2 - n_4^2{\beta_1}^2}, n_3\pi \neq n_4\beta_2 \\ \frac{2n_4\beta_2 \cos(n_4\theta_k) - \sin(n_4\theta_k) + \sin(n_4(\theta_k+\beta_2))}{4n_4}, \ n_3\pi = n_4\beta_2 \end{cases} \tag{A72}$$

$$g_t(n_3, n_4, k) = \begin{cases} \frac{n_4^2 {\beta_2}^2 \left[-\cos(n_4\theta_k) + (-1)^{n_3} \cos(n_4(\theta_k+\beta_2))\right]}{n_3^2\pi^2 - n_4^2{\beta_2}^2}, n_3\pi \neq n_4\beta_2 \\ \frac{2n_4\beta_2 \sin(n_4\theta_k) + \cos(n_4\theta_k) - \cos(n_4(\theta_k+\beta_2))}{4n_4}, \ n_3\pi = n_4\beta_2 \end{cases} \tag{A73}$$

$$f_f(n_5, n_4, l) = \begin{cases} \frac{n_4^2 \gamma^2 \left[\sin(n_4\theta_l) + (-1)^{n_5+1} \sin(n_4(\theta_l+\gamma))\right]}{n_5^2\pi^2 - n_4^2\gamma^2}, n_5\pi \neq n_4\gamma \\ \frac{2n_4\gamma \cos(n_4\theta_l) - \sin(n_4\theta_l) + \sin(n_4(\theta_l+\gamma))}{4n_4}, \ n_5\pi = n_4\gamma \end{cases} \tag{A74}$$

$$g_f(n_5, n_4, l) = \begin{cases} \frac{n_4^2 \gamma^2 \left[-\cos(n_4\theta_l) + (-1)^{n_5} \cos(n_4(\theta_l+\gamma))\right]}{n_5^2\pi^2 - n_4^2\gamma^2}, n_5\pi \neq n_4\gamma \\ \frac{2n_4\gamma \sin(n_4\theta_l) + \cos(n_4\theta_l) - \cos(n_4(\theta_l+\gamma))}{4n_4}, \ n_5\pi = n_4\gamma \end{cases} \tag{A75}$$

$$f_f(n_5, n_6, l) = \begin{cases} \frac{n_6^2 \gamma^2 \left[\sin(n_6\theta_l) + (-1)^{n_5+1} \sin(n_6(\theta_l+\gamma))\right]}{n_5^2\pi^2 - n_6^2\gamma^2}, n_5\pi \neq n_6\gamma \\ \frac{2n_6\gamma \cos(n_6\theta_l) - \sin(n_6\theta_l) + \sin(n_6(\theta_l+\gamma))}{4n_6}, \ n_5\pi = n_6\gamma \end{cases} \tag{A76}$$

$$g_f(n_5, n_6, l) = \begin{cases} \frac{n_6^2 \gamma^2 \left[-\cos(n_6\theta_l) + (-1)^{n_5} \cos(n_6(\theta_l+\gamma))\right]}{n_5^2\pi^2 - n_6^2\gamma^2}, n_5\pi \neq n_6\gamma \\ \frac{2n_6\gamma \sin(n_6\theta_l) + \cos(n_6\theta_l) - \cos(n_6(\theta_l+\gamma))}{4n_6}, \ n_5\pi = n_6\gamma \end{cases} \tag{A77}$$

$$f_s(n_7, n_6, m) = \begin{cases} \frac{n_6^2 \delta^2 \left[\sin(n_6\theta_m) + (-1)^{n_7+1} \sin(n_6(\theta_m+\delta))\right]}{n_7^2\pi^2 - n_6^2\delta^2}, n_7\pi \neq n_6\delta \\ \frac{2n_6\delta \cos(n_6\theta_m) - \sin(n_6\theta_m) + \sin(n_6(\theta_m+\delta))}{4n_6}, \ n_7\pi = n_6\delta \end{cases} \tag{A78}$$

$$g_s(n_7, n_6, m) = \begin{cases} \frac{n_6^2 \delta^2 \left[-\cos(n_6\theta_m) + (-1)^{n_7} \cos(n_6(\theta_m+\delta))\right]}{n_7^2\pi^2 - n_6^2\delta^2}, n_7\pi \neq n_6\delta \\ \frac{2n_6\delta \sin(n_6\theta_m) + \cos(n_6\theta_m) - \cos(n_6(\theta_m+\delta))}{4n_6}, \ n_7\pi = n_6\delta \end{cases} \tag{A79}$$

$F(n_1, n_2)$ can be further simplified as:

$$F(n_1, n_2) = \begin{cases} \frac{\frac{n_1\pi}{\alpha}\left[(-1)^{n_2} \sin\left(\frac{n_1\pi(\alpha+\beta_1)}{2\alpha}\right) - \sin\left(\frac{n_1\pi(\alpha-\beta_1)}{2\alpha}\right)\right]}{\left(\frac{n_1\pi}{\alpha}\right)^2 - \left(\frac{n_2\pi}{\beta_1}\right)^2}, & \frac{n_1\pi}{\alpha} \neq \frac{n_2\pi}{\beta_1} \\ \frac{\beta_1}{2}\cos\left(\frac{n_2\pi}{2\beta_1}(\beta_1 - \alpha)\right), & \frac{n_1\pi}{\alpha} = \frac{n_2\pi}{\beta_1} \end{cases} \tag{A80}$$

References

1. Niu, S.; Chau, K.T.; Jiang, J.Z.; Liu, C. Design and Control of a New Double-Stator Cup-Rotor Permanent-Magnet Machine for Wind Power Generation. *IEEE Trans. Magn.* **2007**, *43*, 2501–2503. [CrossRef]
2. Gul, W.; Gao, Q.; Lenwari, W. Optimal Design of a 5-MW Double-Stator Single-Rotor PMSG for Offshore Direct Drive Wind Turbines. *IEEE Trans. Ind. Appl.* **2020**, *56*, 216–225. [CrossRef]
3. Fan, D.; Quan, L.; Zhu, X.; Xiang, Z.; Que, H. Airgap-Harmonic-Based Multilevel Design and Optimization of a Double-Stator Flux-Modulated Permanent-Magnet Motor. *IEEE Trans. Ind. Electron.* **2021**, *68*, 10534–10545. [CrossRef]

4. Yu, J.; Liu, C.; Song, Z.; Zhao, H. Permeance and Inductance Modeling of a Double-Stator Hybrid-Excited Flux-Switching Permanent-Magnet Machine. *IEEE Trans. Transp. Electrif.* **2020**, *6*, 1134–1145. [CrossRef]
5. Asef, P.; Perpina, R.B.; Moazami, S.; Lapthorn, A.C. Rotor Shape Multi-Level Design Optimization for Double-Stator Permanent Magnet Synchronous Motors. *IEEE Trans. Energy Convers.* **2019**, *34*, 1223–1231. [CrossRef]
6. Roth, C.; Milde, F.; Trebbels, D.; Schmidt, J.; Doppelbauer, M. A Stator with Offset Segments and a Double Stator Design for the Reduction of Torque Ripple of a Switched Reluctance Motor. *IEEE Trans. Energy Convers.* **2022**, *37*, 1233–1240. [CrossRef]
7. Toba, A.; Lipo, T.A. Generic torque-maximizing design methodology of surface permanent-magnet vernier machine. *IEEE Trans. Ind. Appl.* **2000**, *36*, 1539–1546. [CrossRef]
8. Zhao, H.; Liu, C.; Song, Z.; Wang, W. Exact Modeling and Multiobjective Optimization of Vernier Machines. *IEEE Trans. Ind. Electron.* **2021**, *68*, 11740–11751. [CrossRef]
9. Li, D.; Qu, R.; Lipo, T.A. High-Power-Factor Vernier Permanent-Magnet Machines. *IEEE Trans. Ind. Appl.* **2014**, *50*, 3664–3674. [CrossRef]
10. Boughrara, K.; Ibtiouen, R.; Zarko, D.; Touhami, O.; Rezzoug, A. Magnetic Field Analysis of External Rotor Permanent-Magnet Synchronous Motors Using Conformal Mapping. *IEEE Trans. Magn.* **2010**, *46*, 3684–3693. [CrossRef]
11. Hemeida, A.; Lehikoinen, A.; Rasilo, P.; Vansompel, H.; Belahcen, A.; Arkkio, A.; Sergeant, P. A Simple and Efficient Quasi-3D Magnetic Equivalent Circuit for Surface Axial Flux Permanent Magnet Synchronous Machines. *IEEE Trans. Ind. Electron.* **2019**, *66*, 8318–8333. [CrossRef]
12. Zhao, H.; Chau, K.T.; Yang, T.; Song, Z.; Liu, C. A Novel Quasi-3D Analytical Model for Axial Flux Motors Considering Magnetic Saturation. *IEEE Trans. Energy Convers.* **2022**, *37*, 1358–1368. [CrossRef]
13. Zhao, H.; Liu, C.; Song, Z.; Wang, W. Analytical Modeling of a Double-Rotor Multiwinding Machine for Hybrid Aircraft Propulsion. *IEEE Trans. Transp. Electrif.* **2020**, *6*, 1537–1550. [CrossRef]
14. Oner, Y.; Zhu, Z.Q.; Wu, L.J.; Ge, X.; Zhan, H.; Chen, J.T. Analytical On-Load Subdomain Field Model of Permanent-Magnet Vernier Machines. *IEEE Trans. Ind. Electron.* **2016**, *63*, 4105–4117. [CrossRef]
15. Wu, L.; Zhu, M.; Wang, D.; Fang, Y. A Subdomain Model for Open-Circuit Field Prediction in Dual-Stator Consequent-Pole Permanent Magnet Machines. *IEEE Trans. Magn.* **2019**, *55*, 1–12. [CrossRef]
16. Cheng, M.; Han, P.; Du, Y.; Wen, H. General Airgap Field Modulation Theory for Electrical Machines. *IEEE Trans. Ind. Electr.* **2017**, *64*, 6063–6074. [CrossRef]
17. Gysen, B.L.J.; Meessen, K.J.; Paulides, J.J.H.; Lomonova, E.A. General Formulation of the Electromagnetic Field Distribution in Machines and Devices Using Fourier Analysis. *IEEE Trans. Magn.* **2010**, *46*, 39–52. [CrossRef]
18. Lubin, T.; Mezani, S.; Rezzoug, A. 2-D Exact Analytical Model for Surface-Mounted Permanent-Magnet Motors with Semi-Closed Slots. *IEEE Trans. Magn.* **2011**, *47*, 479–492. [CrossRef]
19. Zhao, H.; Liu, C.; Song, Z.; Liu, S.; Lubin, T. Analytical Model for Magnetic-Geared Double-Rotor Machines and Its d–q-Axis Determination. *IET Electric. Power Appl.* **2020**, *14*, 175–183. [CrossRef]